

研究課題名：時分割X線回折法によるスメクティック液晶の動的構造解析

研究代表者：関澤 和子 (日本大学・理工学部・物理学科)

研究従事者：高橋 由美子 (日本大学・理工学部・物理学科)

共同研究者：飯田 厚夫 (KEK, PF)

高野 良紀 (日本大学・理工学部・物理学科)

高瀬 浩一 (日本大学・理工学部・物理学科)

【研究目的】

液晶に代表されるソフトマターは外力に対する応答性が良く、小さな外場で大きな構造変化を示す。ソフトマターの空間的・時間的変化の詳細を検討し、その秩序形成過程、相転移機構等を解明するためには、構造変化の過程を実時間で直接観察することが望ましい。そこでFELを用いたX線(パラメトリックX線)のパルス性を活用した時分割X線回折光学系を構築し、スメクティック液晶の電場応答など、ソフトマターの構造変化過程を観察する手法を確立することを目的とした。

【研究概要】

(1) 実験準備

パラメトリックX線を用いた時分割X線回折法の開発準備として、液晶の電場応答が時分割X線回折法によって観察可能であることを確認するため、高エネルギー加速器研究機構、放射光研究施設BL-4Aにおいて実験を行った。

実験には時分割マイクロビームX線回折光学系を用いた。本装置は報告者らが開発したものである。偏向電磁石からの連続X線を多層膜分光器により単色化(8 keV)し、Kirkpatrick-Baez型光学素子により集光して試料位置でのビームサイズが約 $3 \times 4 \mu\text{m}^2$ 以下になるよう調整している。角度発散は水平、垂直方向とも1.0 mrad程度、フォトンフラックスは照射損傷を防ぐため 10^8 photons/s程度で使用している。

使用した強誘電性液晶では5ヘルツの三角波に追従して層構造が変化することを確認できた。また、実験のために必要とされる試料ステージの回転・並進軸や試料電場作製方法など、必要とされる基本的な実験条件を把握することができた。

(2) パラメトリックX線を用いた光学系の開発

Si単結晶から発生したパラメトリックX線は指向性が高く準単色光であるので、これを直接試料に照射し、回折X線を得ることで高分解能測定が可能である。このため、実験ホール内のパラメトリックX線取り出し口近傍に設置されたゴニオメータを用い、粉末X線回折光学系で基礎データを収集した。X線エネルギーは10 keV、13.5 keVとした。検出器にはポラロイド・フィルム、CCD、シンチレーション・カウンタ等を用いた。試料が単結晶である場合はシャープな回折線(ロッキングカーブ半価幅で 0.003° 程度)が得られることが早川らによって報告されている。しかし多結晶試料においては回折プロファイルを得るに至っていない。検出器がポラロイド・フィルム、CCDの場合には感度の不足、言い換えれば回折X線の強度不足が主要な原因の一つであると考えられる。また、シンチレーション・カウンタでは回折角 20° 以下で極めて高いバックグラウンドが検出され、回折線が低角度に現れる液晶試料には大きな問題となる。バックグラウンドは中性子線、 γ 線を

多く含んでいると思われるが、現在線質の調査を行っている。バックグラウンドの性質が明らかになれば適切な遮蔽やミラー、PHA、ディスクリミネータの使用等によって効果的に除去できる。シンチレーション・カウンタは広いエネルギー範囲で高感度を保ち、 $\Delta E =$ 数 keV程度であるがエネルギー分解能を持つのでパラメトリックX線の広い応用範囲に対して有効である。よってバックグラウンドを低減しS/Nを向上させることによりシンチレーション・カウンタを検出器とする光学系の確立を目指す。

また、輝度の向上を図るため、楕円ミラーのKirkpatrick-Baezシステムによる集光を行う予定であり、調整が進んでいる。集光により輝度は約 10^4 倍になると見積もられているので、十分な回折X線強度が期待できる。このため、集光系後方に試料をセットする光学系の構築も行っている。集光後のビームサイズは $10 \times 10 \mu\text{m}^2$ 程度となるため、試料軸の交差精度やビーム位置の検出機構等を考慮する必要がある。

これらの基本的光学系を確立したのち、光源のマクロパルスに同期した時分割測定系を付加する予定である。

【まとめ】

液晶の電場応答などソフトマターのダイナミクスを研究する手段として時分割X線回折法が有効であることが確認できた。今後はパラメトリックX線を用いた時分割X線回折光学系を早期に確立し、液晶研究に適用すると共に応用範囲を広げて行く。

【研究業績等】

・ 発表論文

- (1) Atsuo Iida, Yumiko Takahashi, Yoichi Takanishi, Toyokazu Ogasawara, Michi Nakata, Ken Ishikawa and Hideo Takezoe (2005) Dynamic and microscopic X-ray characterization of a compound chevron layer in electroclinic liquid crystals contributed to *Liquid Crystals*
- (2) Yumiko Takahashi, Atsuo Iida, Yoichi Takanishi, Toyokazu Ogasawara, Michi Nakata, Ken Ishikawa and Hideo Takezoe (2003) Dynamic local layer response of surface stabilize ferroelectric liquid crystals to high electric field by time-resolved x-ray micro-diffraction *Phys. Rev. E* **67**, 051706-1 – 051706-10
- (3) Yumiko Takahashi, Atsuo Iida, Yoichi Takanishi, Toyokazu Ogasawara, Michi Nakata, Ken Ishikawa and Hideo Takezoe (2004) Temperature and electric field dependences of the local layer structure in anti-ferroelectric liquid crystals measured by X-ray micro-diffraction. *Ferroelectrics*, **311**, 41-50
- (4) A.Iida, Y.Takanishi, Y.Takahashi, M.Nakata, K.Ishikawa and H. Takezoe (2002) Observation of dynamic local layer response of smectic liquid crystals by X-ray micro-diffraction *Acta Cryst. A* **58** (Suppl.), C337
- (5) Y.Takahashi, A.Iida, Y.Takanishi, T. Ogasawara and H. Takezoe (2001) Time resolved X-ray micro-diffraction measurements of the dynamic local layer response to electric field in antiferroelectric liquid crystals *Nucl. Instr. and Meth. A* **467-468**, 1001-1004

・ 学会発表

- (1) 高橋由美子 (2004) (反) 強誘電性液晶における局所構造の電場応答— 一時分割マイクロビーム X線回折法による動的構造解析— 第48回理工学部学術講演会 (理工学部船橋校舎)
- (2) 飯田 厚夫, 高橋 由美子, 高西 陽一, 中田未知, 石川 謙, 竹添 秀男 (2004) 電傾効果における層構造と分子配向の動的微小領域X線回折法による評価 2004年日本液晶学会討論会 (名古屋大学, 名古屋)
- (3) Atsuo Iida, Yumiko Takahashi, Yoichi Takanishi Michi Nakata, Ken Ishikawa and Hideo Takezoe (2004) Dynamic local layer structure in the electroclinic effect : Time-resolved X-ray micro-diffraction 20th International Liquid Crystal Conference (Ljubljana, Slovenia)
- (4) 飯田厚夫, 高橋由美子, 高西陽一, 中田未知, 利光めぐみ, 石川謙, 竹添秀男 (2004) 強誘電液晶のSmA相電傾効果における局所層構造の動的解析 第17回日本放射光学会年回・放射光科学合同シンポジウム (つくば国際会議場, つくば)
- (5) 飯田厚夫, 高橋由美子, 高西陽一, 中田未知, 利光めぐみ, 石川謙, 竹添秀男 (2003) SmA相電傾効果における局所層構造の動的解析 2003年日本液晶学会討論会 (青森市文化会館, 青森)
- (6) Yumiko Takahashi, Atsuo Iida, Yoichi Takanishi, Michi Nakata, Ken Ishikawa and Hideo Takezoe (2003) Static and dynamic local layer structure under the electric field in antiferroelectric liquid crystal measured by X-ray micro-diffraction 9th International Conference on Ferroelectric Liquid Crystals (Trinity College, University of Dublin, Dublin)
- (7) Atsuo Iida, Yumiko Takahashi, Yoichi Takanishi, Michi Nakata and Hideo Takezoe (2003) Dynamic local layer response of smectic liquid crystals under the ac electric field by time-resolved X-ray micro-diffraction 8th International Conference on Synchrotron Radiation Instrumentation (Yerba

Buena Arts Center, San Francisco)

- (8) 高橋由美子, 飯田厚夫, 高西陽一, 中田未知, 利光めぐみ, 石川謙, 竹添秀男 (2003) スメクティック液晶電傾効果における局所層構造応答—マイクロビームX線回折法— 第16回放射光学会年会・放射光科学合同シンポジウム (イーグレ姫路, 姫路)
- (9) 高橋由美子, 飯田厚夫, 高西陽一, 中田未知, 利光めぐみ, 石川謙, 竹添秀男 (2002) 電傾効果におけるSmA相の局所層構造の応答 2002年日本液晶学会討論会 (奈良県新公会堂, 奈良)
- (10) 高橋由美子, 飯田厚夫, 高西陽一, 小笠原豊和, 中田未知, 石川謙, 竹添秀男 (2002) マイクロビームによる(反)強誘電性液晶層構造の不可逆的・可逆的電場応答 第15回放射光学会年会・放射光科学合同シンポジウム (東京大学物性研究所, 柏)
- (11) 高橋由美子, 飯田厚夫, 高西陽一, 小笠原豊和, 中田未知, 石川謙, 竹添秀男 (2001) 強誘電/反強誘電性液晶における層構造の電場応答と光学応答 2001年日本液晶学会討論会 (大宮ソニックシティ, さいたま)
- (12) 高橋由美子, 飯田厚夫, 高西陽一, 小笠原豊和, 石川謙, 竹添秀男 (2001) 反強誘電性液晶および強誘電性液晶における局所層構造の動的電場応答の対応 第48回 応用物理学関係連合講演会 (明治大学, 東京)
- (13) 高橋由美子, 飯田厚夫, 高西陽一, 小笠原豊和, 石川謙, 竹添秀男 (2001) マイクロビームによる反強誘電性液晶層構造の過渡的電場応答 第14回 放射光学会年回・放射光科学合同シンポジウム (広島大学, 広島)

Dynamic local-layer response of surface-stabilized ferroelectric liquid crystals to a high electric field by time-resolved x-ray microdiffraction

Yumiko Takahashi*

The Graduate University for Advanced Studies, 1-1 Oho Tsukuba, Ibaraki 305-0801, Japan

Atsuo Iida

Photon Factory, Institute of Materials Structure Science, High Energy Accelerator Research Organization, 1-1 Oho Tsukuba, Ibaraki 305-0801, Japan

Yoichi Takanishi, Toyokazu Ogasawara, Michi Nakata, Ken Ishikawa, and Hideo Takezoe

Department of Organic and Polymeric Materials, Tokyo Institute of Technology, O-okayama Meguro-ku, Tokyo 152-8552, Japan

(Received 15 August 2002; revised manuscript received 20 February 2003; published 23 May 2003)

Time-resolved synchrotron x-ray microdiffraction measurements have directly revealed the dynamic local-layer response to the high electric field in a surface-stabilized ferroelectric liquid crystal. The irreversible layer transformation under the increasing electric field is found to consist of two stages; the initial vertical chevron structure transforms to the alternate vertical and horizontal chevrons and, with increasing field, the chevron angle decreases and the horizontal chevron structure develops. The time-resolved microdiffraction measurement has clarified the detailed reversible layer transformation between the mostly horizontal chevron at the high field and the so-called quasibookshelf at the low field during the ac field application. The transient layer response time is about 0.1–0.2 and 0.3–0.4 ms for falling and rising edges, respectively, and is slightly longer than the optical response time. The layer transformation is discussed in terms of electric torque and surface anchoring. The local-layer response in the antiferroelectric liquid crystal is also discussed for comparison.

DOI: 10.1103/PhysRevE.67.051706

PACS number(s): 61.30.–v

I. INTRODUCTION

The local-layer structures of ferroelectric liquid crystals (FLCs) and antiferroelectric liquid crystals (AFLCs) and their layer response to an electric field have attracted much attention both from display device applications and fundamental physics [1,2]. When the smectic-A (SmA) phase is cooled down to the chiral smectic-C (SmC*) phase, the reduction of the layer spacing is compensated by a vertical chevron (v-chevron) structure in a surface-stabilized cell [2–7]. Optical and electro-optical phenomena could be interpreted in terms of this v-chevron structure and its modification. Under the high electric field, an irreversible layer transition from the initial v chevron to the so-called quasibookshelf structure was observed in both surface-stabilized AFLC and FLC cells [9–11]. When observed with a polarized optical microscope, the quasibookshelf structure often accompanies the stripe texture that degrades the optical contrast for display applications. The stripe texture has been discussed with regard to the horizontal chevron (h-chevron) structure [12]. The h chevron is realized due to the interaction between the applied electric field and the spontaneous polarization of the molecule. The h-chevron structures, however, are not restricted to the SmC* under the high-field treatment, but also they were found in the FLC without the field treatment [13] and in the electroclinic effect in the SmA phase [12,14,15]. Recently, the v chevron to quasibookshelf

transition has been also studied in detail by x-ray small angle scattering in relation to the ferroelectric, ferrielectric, and antiferroelectric phases as a function of temperature and the electric field [16–19]. Since the h chevron is a laterally inhomogeneous layer structure in a cell, a spatially resolved x-ray technique is indispensable to directly determine the local-layer structure. Small angle x-ray scattering with a synchrotron x-ray microbeam is the direct microscopic technique and has proven to be quite effective for the characterization of smectic liquid crystals [20–25].

Obviously, for the study of the electro-optical behavior of the FLCs and AFLCs, it is important to directly investigate the dynamic as well as the static layer structure of the v and h chevrons in detail. The x-ray experiments having a millisecond (ms) to microsecond (μ s) time resolution for the liquid crystal layer determination, however, have been limited in number. The layer responses from a few tens of microseconds to sub-milliseconds were observed even under the relatively low electric field of a symmetric bipolar pulse [26,27]. Recently, the local-layer structure in the AFLCs and its response to the applied electric field were successfully revealed by time-resolved synchrotron x-ray microdiffraction [28,29].

In this paper, the local-layer structure of the FLCs and its response to the electric field are investigated to reveal the dynamic interaction of the field with the local-layer structure by x-ray small angle scattering with a few μ m spatial resolution and a few tens of μ s time resolution. Furthermore, the orthogonal ω - and χ -angular dependences of diffracted intensities are fully utilized to study the field-induced layer transformation. Simultaneous observation of the optical response with the x-ray measurement also makes it possible to discuss the relationship between the molecular and the layer re-

*Present address: Nihon University, Surugadai, Kanda, Chiyodaku, Tokyo 101-8308, Japan.

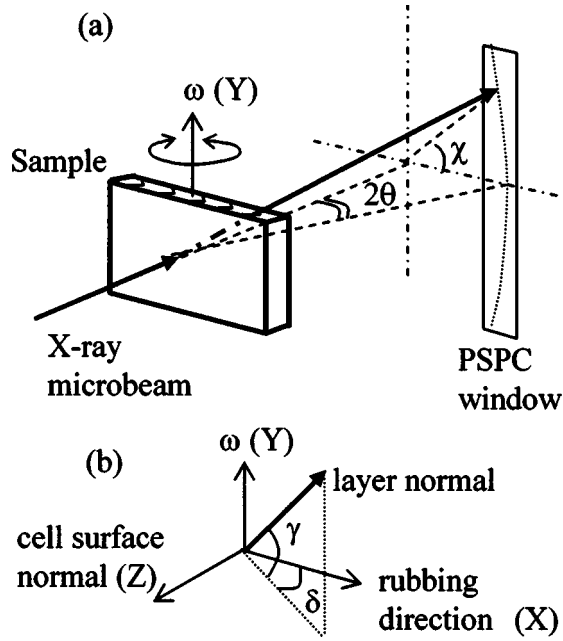


FIG. 1. (a) Experimental setup for synchrotron x-ray microbeam diffraction. (b) Sample coordinates for the smectic layer normal. The angle δ is the tilt angle or the vertical chevron angle. γ is the in-plane deflection angle or the horizontal chevron angle when the chevron structure is periodic.

sponse. The quasistatic and transient layer transformations for the triangular-form and the step-form electric fields, respectively, are reported. The results are also discussed in relation to the AFLC layer response.

II. EXPERIMENT

The sample was TK-C101 (Chisso) [23] sandwiched between ITO-coated glass plates (150 μm thick) rubbed on one side after coating a polyimide alignment film. The phase sequence of TK-C101 is iso(80°C) N^* (70°C)SmA(56°C)SmC*. The experiments were performed in the SmC* phase at room temperature. Most of the experiments were carried out with one-side rubbing cells, which is the same alignment condition as previous AFLC experiments [28,29]. The cell gap was about 5–8 μm . For comparison, an AFLC sample (S)-TFMHPOBC [4-(1-trifluoromethyl heptyloxy-carbonyl)phenyl 4'-octyloxy-biphenyl-4-carboxylate] was also measured at the same sample temperature of $T_c - 10^\circ$ as previous experiments [28,29], where T_c is the phase transition temperature from SmA to SmC*_A (109°C).

The x-ray diffraction experiments were carried out on beam line 4A at the Photon Factory (PF). The experimental detail has been already reported in the previous paper [28], so only a brief description is given here. The beam size was about 3(h) \times 4(v) μm^2 and the angular divergence of the incident beam was about 1.0 mrad both in the horizontal and in the vertical direction. The incident x-ray energy was 8 keV (1.55 Å). The diffraction geometry is schematically shown in Fig. 1(a). The rubbing direction was set horizontally. The χ -intensity distribution (χ profile) on a position sensitive

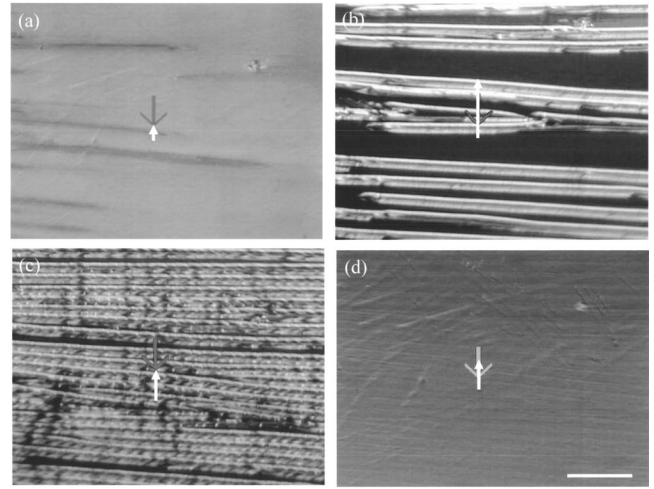


FIG. 2. Polarized optical micrographs of textures of the initial stage before field application (a), ± 18 V (b), ± 28 V (c), and ± 60 V (d) under the triangular wave form (5 Hz). The sample was TK-C101. The cell thickness was about 7.5 μm . The measurement was done at room temperature. The rubbing direction was set horizontally. White arrows show the direction and the region of the x-ray measurement shown in Fig. 3. A scale mark is 100 μm . (Weak gray arrows show points of measurements during the experiments.)

proportional counter was collected simultaneously. The ω -scan intensity profile (ω profile) was obtained by rotating the sample around a vertical axis (Y). The ω intensity is the integrated intensity with respect to χ in the present paper. No absorption correction for the cell glass plates was made. The layer deflection angles δ and γ are defined in Fig. 1(b).

The optical response was obtained by a photomultiplier attached to an *in situ* polarized microscope during the x-ray measurement, though the optical measurement area was about 100 μm in diameter and was much larger than the x-ray microbeam size.

A triangular-form (5 Hz, ± 1 – ± 65 V) or a step-form (25–100 Hz, ± 45 – ± 65 V) electric field was applied to the sample. The time-resolved ω profile and χ profile were obtained with an MCS (multichannel scaler) mode and a gated MCA (multichannel analyzer) mode, respectively. A minimum dwell time for the MCS mode was 10 μs . In the gated MCA mode, the χ profiles at eight sampling points in one cycle of the applied field were collected with a minimum time resolution of 10 μs . MCS and MCA data were summed within a measurement time.

III. RESULTS

A. Time integrated spatial distribution of the diffraction profile

The time integrated spatial distribution of the x-ray diffraction profile from TK-C101 was measured as a function of an applied voltage (Fig. 3) together with the *in situ* observation of the texture by a polarized optical microscope (Fig. 2).

Figures 3(1-a) and 3(1-b) show series of ω and χ profiles, respectively, across the narrow wall at an initial state before the field application. The v-chevron structure (peaks at $\omega = \pm 21^\circ$) is clearly seen in Fig. 3(1-a). The peaks that ap-

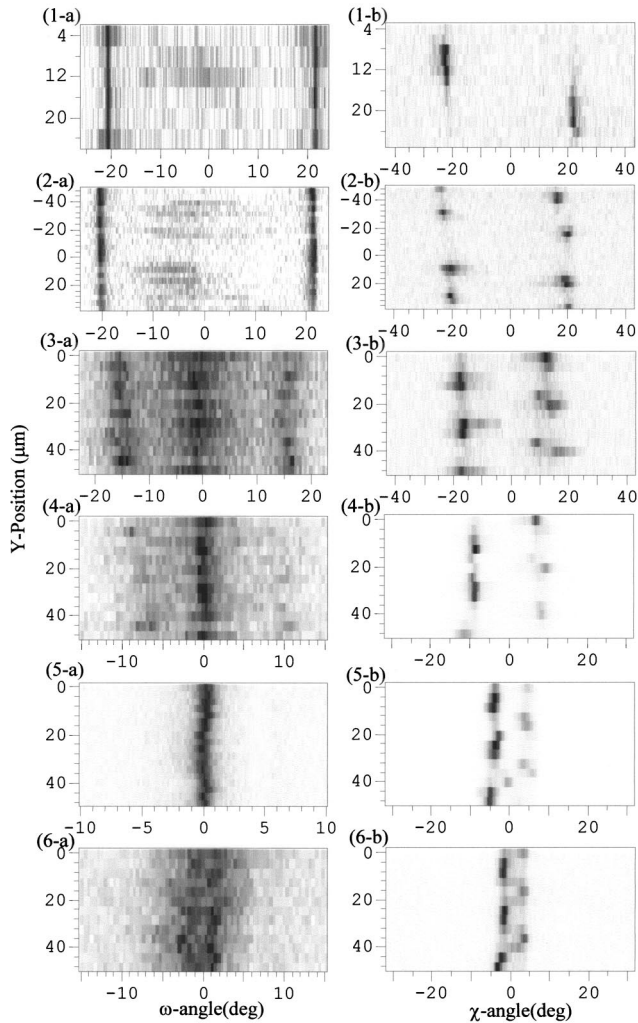


FIG. 3. Series of ω profiles (a) and χ profiles (b) as a function of the vertical position (Y direction). (1-a) and (1-b) were obtained before the field application. (2-a) and (2-b), (3-a) and (3-b), (4-a) and (4-b), and (5-a) and (5-b) were obtained during the triangular field of ± 18 , ± 30 , ± 40 , and ± 60 V, respectively. (6-a) and (6-b) were obtained after turning off the field. The χ profiles were obtained at $\omega = 0^\circ$ except for (2-b) where $\omega = -5.8^\circ$ (see text). The scanning step in the Y direction was $4 \mu\text{m}$. The darker part corresponds to the higher diffracted intensity. X-ray intensities were normalized by the highest intensity in each figure.

peared in χ profiles [Fig. 3(1-b)] are due to a pair of the narrow wall of a zigzag defect observed in Fig. 2(a). Thus, the v-chevron angle (δ) and the in-plane deflection angle at the narrow wall (γ) are 21° and 22° , respectively.

When the triangular electric field with a frequency of 5 Hz was applied to the sample, most of the narrow walls in the view field disappeared up to ± 5 V [8] and the new line defect (needle defect [20,23], hereafter) appeared above ± 10 V. The needle defect usually appeared from a broad wall, the tip of a narrow wall or a spacer edge. At ± 18 V [Fig. 2(b)], the needle defect develops and the so-called stripe texture is formed. A series of the ω profiles [Fig. 3(2-a)] shows broad but weak peaks (ω -bookshelf components, hereafter) between the v-chevron peaks. The χ -intensity distribution [Fig.

3(2-b)] obtained at $\omega = -5.8^\circ$ (peak of ω -bookshelf component) shows the alternate intensity variation between the low and high angles indicating the nearly periodic needle-defect formation (h-chevron growth). The angles δ and γ are almost the same as in the initial state.

By increasing the applied voltage, the needle defect further develops and covers the whole area as shown in Fig. 2(c). It is also noted that dense focal conics appear in the needle defect (or stripe) reflecting the strain field. The intensity modulation in Figs. 3(3-a) and 3(3-b) is about $8\text{--}10 \mu\text{m}$ in period, which is close to the cell thickness. Above the applied voltage of around ± 30 V, the spatial period of the χ -profile modulation is almost unchanged. The angles δ and γ become small and the FWHM (full width at half maximum) of the v-chevron peak in the ω profile slightly increases up to 1° from the initial one (about 0.4°) indicating the strain introduction.

Up to ± 50 V, the stripe texture progressively covers the whole sample area and the focal conics density increases. With increasing applied voltage, the angles δ and γ become small and the v-chevron intensity further becomes weak as shown in Figs. 3(4-a) and 3(4-b). It is noted, however, that the v-chevron structure still remains at this stage.

Above ± 50 V, the contrast of the stripe texture becomes very weak and focal conics disappear [Fig. 2(d)]. The ω profiles obtained at ± 60 V [Fig. 3(5-a)], which is the highest applied voltage for this sample show a sharp peak near $\omega = 0^\circ$ and are almost independent of the position. The χ profiles [Fig. 3(5-b)], however, show the alternate intensity distribution from position to position. The angle γ decreases down to 5° on an average.

When the electric field is turned off, the ω profile becomes broad and the angle γ becomes small (3°) as shown in Figs. 3(6-a) and 3(6-b). Compared to the initial state, the local-layer structure is irreversibly transformed. The ω profile looks like the quasibookshelf or the strongly modified v-chevron structure.

A series of time integrated spatial distributions in Fig. 3 has revealed the local-layer structure in a microscopic scale. The detail of the layer structure, however, seems to depend on the sample and the history of the field application. Figure 4 shows the other typical ω and χ profiles from a different sample for the high applied field [Figs. 4(a) and 4(b)] and after turning off the field [Figs. 4(c) and 4(d)]. The ω profiles at the high voltage (± 50 V) show the single peak [Fig. 4(a)] similar to Fig. 3(5-a), while the χ profiles in Fig. 4(b) are broader than those in Fig. 3(5-b) and the periodic structure is not so clear. After turning off the field, this type of the sample shows a single peak in the χ profile [Fig. 4(d)] in contrast to the alternate two peaks shown in Fig. 3(6-b), while the ω profile [Fig. 4(c)] is similar to Fig. 3(6-a). For all these differences among samples, the local-layer structure after turning off the field is characterized by the broadening of the ω profile and the narrowing of the chevron angle γ or a single peak in the χ profile. Hereafter, the layer structures in Figs. 3 and 4 are referred to as the type *D* and type *S*, indicating the double and single peaks in the χ profile after turning off the field, respectively.

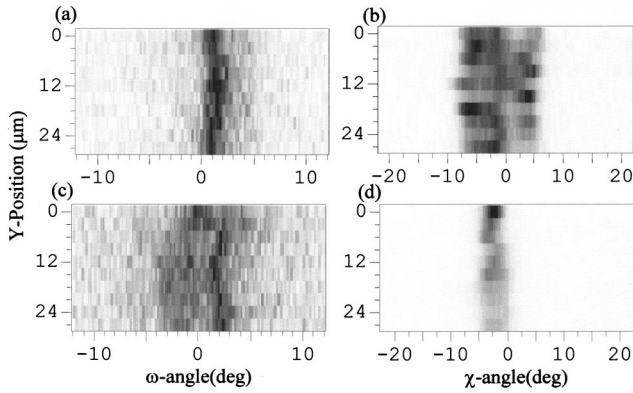


FIG. 4. Series of ω profiles [(a) and (c)] and χ profiles at $\omega = 0^\circ$ [(b) and (d)] as a function of the vertical position across the stripe. Under the ± 50 V field application [(a) and (b)] and after turning off the field [(c) and (d)]. The sample thickness was $6 \mu\text{m}$.

To summarize the layer deformation process, the ω and χ profiles in Fig. 3 are summed for Y positions (temporally and spatially integrated profiles, Fig. 5). The irreversible v chevron to the quasibookshelf transformation in ω profiles [Fig. 5(a)] well agrees with previous x-ray diffraction experiments [8,10,17,19], while the simultaneous χ -profile measurement clearly indicates various stages of the h-chevron formation.

Finally, the layer transformation having a long relaxation time is mentioned. Uppermost profiles in Fig. 5 (long) are

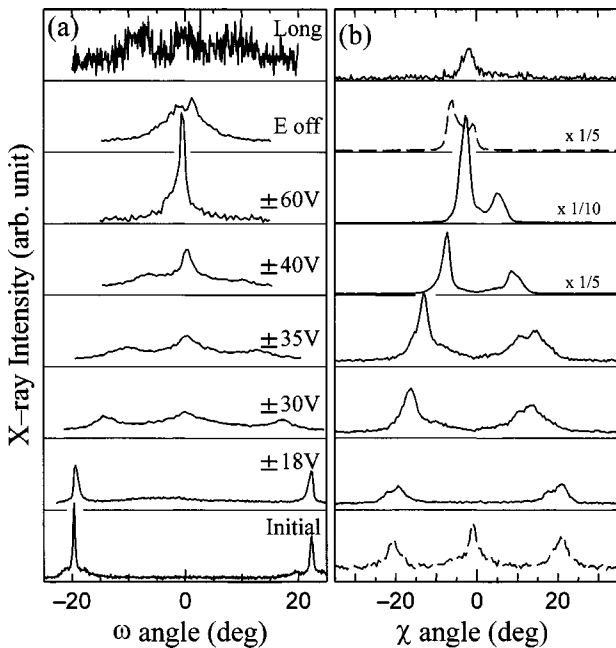


FIG. 5. Summary of the time integrated ω profile (a) and χ profile (b). From ± 18 V to E off (after turning off the electric field), the diffracted intensities were obtained by integrating over the position from series of ω and χ profiles (Fig. 3). For the initial profile, the χ profile (broken line) was measured during the ω -profile measurement at the center of the narrow wall (integrated over ω angle). Uppermost profiles (long) were obtained from a different sample at a single position (no spatial integration) after a long interval without electric field application.

obtained after a long time interval (about four months) without electric field application. Poor statistics are due to the lack of the spatial integration in this case. Multiple broad peaks in the ω profile indicate the partial recovery of the v -chevron structure. The layer relaxation seems to proceed quite slowly.

B. Quasistatic response

The time-resolved experiments under the quasistatic condition were performed with a 5-Hz triangular wave for the sample after the irreversible transition, i.e., time-resolved measurements of Figs. 3(5-a) and 3(5-b). Figures 6(a) and 6(b) show the time-resolved MCS-mode ω profiles from the sample used in Fig. 3 for one cycle of applied voltage (± 60 V amplitude) as a function of time for different positions ($8\text{-}\mu\text{m}$ apart in the Y position). In Fig. 6(a), a single peak near $\omega = 0^\circ$ at the high field shifts to the low angle by about 1° and becomes broad at the low field. In Fig. 6(b), a weak hump appears at the low angle side and it shifts to lower angles with increasing voltage, and the broad double peak appears at low voltage. These two patterns, Figs. 6(a) and 6(b), appeared from position to position in the Y direction alternately. Figure 6(c) shows the ω -profile intensity near $\omega = 0^\circ$ obtained from Fig. 6(b) as a function of the applied voltage (voltage-dependent profile). The intensity has maxima at around ± 30 V and decreases at lower and higher applied voltages. The decrease in the intensity is compensated by the low-angle weak hump at the high field, while, naturally, it is due to the shift and broadening of the ω -profile peak at the low field. The layer response is different from the optical one.

Although Figs. 6(a) and 6(b) are the typical time-resolved ω profiles for the triangular wave, several types of the ω profile seem to appear at the low field from various samples and positions: the asymmetric broad peak [tilted bent bookshelf, Fig. 6(a)], the broad double peak [modified v chevron, Fig. 6(b)] and the symmetric broad peak (quasibookshelf). The common feature of these is the broad profile. It is also noted that the FWHM of the ω profile after turning off the field [Fig. 3(6-a)] is broader than that at 0 V during the ac field application. Therefore, the layer response under the triangular field (5 Hz) is a quasistatic process.

The time-resolved MCA-mode χ profile shows remarkable profile change during the field application. Figures 7(a) and 7(b) are obtained from different samples. In Fig. 7(a), the angular separation of about 10° of the double peak at the high field ($\gamma \sim 5^\circ$) decreases down to 4° – 5° at the low field ($\gamma \sim 2^\circ$) while, in Fig. 7(b), the double peak at the high field changes continuously to the single peak at the low field. Figures 7(a) and 7(b) relate to the type D and type S layer transformations, respectively. In practice, the time dependence of the type S [Fig. 7(b)] is more frequently observed. The positional dependence of the time-resolved χ profile showed the alternate low- and high-angle peaks.

The reversible layer response such as shown in Figs. 6 and 7 started when δ and/or γ became less than $\sim 10^\circ$ or dense focal conics disappeared. Below that voltage, no con-

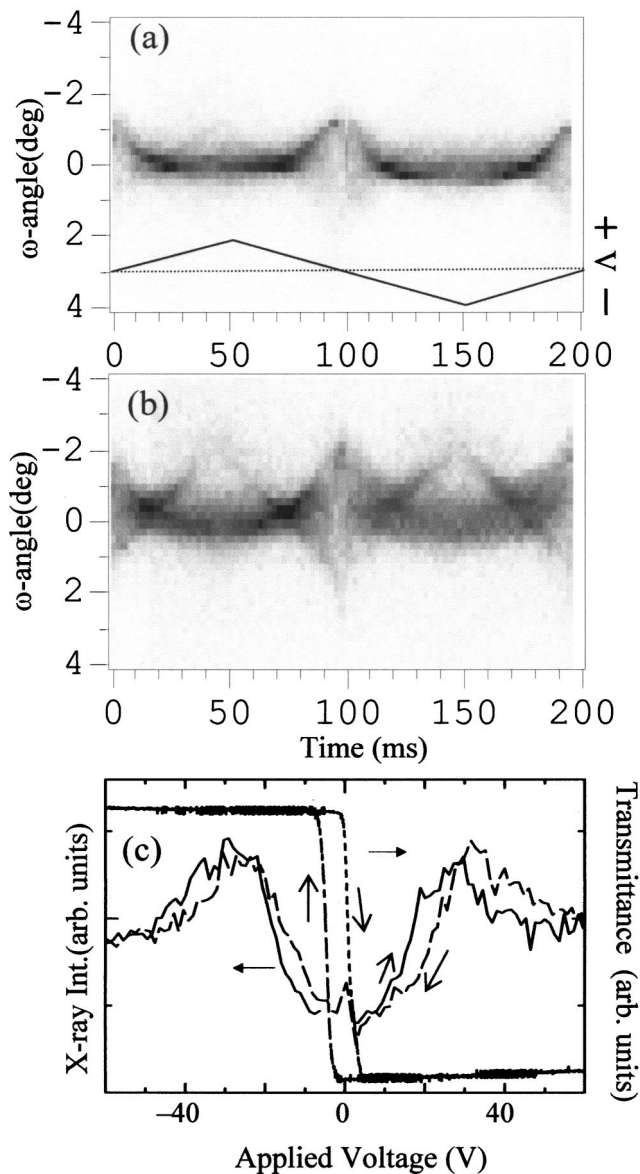


FIG. 6. Time-resolved MCS-mode ω profiles for one cycle of the triangular wave form (5 Hz) [(a) and (b)]. (a) and (b) were obtained from the sample used in Fig. 3 at positions $8 \mu\text{m}$ apart in the Y direction. An inset in (a) shows the wave form applied to the sample. The maximum applied voltage was ± 60 V. The time resolution was 1 ms. The data for the last 2.5% of one cycle are lacking due to the limitation of the timing control procedure for present electronics. (c) The applied voltage dependence of the ω -profile intensity near $\omega = 0^\circ$ (voltage-dependence profile) obtained from (b). The optical transmittance is also shown.

spicuous χ -profile response to the applied field was observed.

From the time-resolved measurement, the quasistatic reversible layer transformation was revealed for the first time.

C. Transient response

The transient layer response was investigated under a step-form electric field (25 Hz, ± 60 V). The time-resolved MCS-mode ω profile for one cycle of the field is shown in

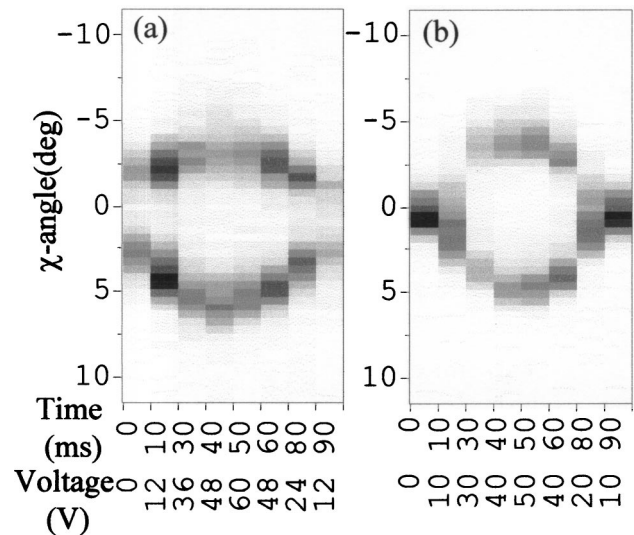


FIG. 7. Time-resolved MCA-mode χ profiles for a half cycle of the triangular wave form [5 Hz, see the inset of Fig. 6(a)]. (a) and (b) were obtained for different samples and the maximum applied voltages were ± 60 and ± 50 V, respectively. Both profiles were obtained near $\omega \sim 0^\circ$. 10 ms time resolution. Note that the sampling times (abscissa) are not at equal intervals.

Fig. 8(a). The ω profiles at the high and low fields, time integrated for 3 ms of Fig. 8(a), are shown in Fig. 8(b). A strong peak near $\omega = 0^\circ$ and weak humps near $\omega = \pm 4^\circ$ at the high field, and a broad single peak at the low field are seen. The time dependent integrated intensity of the ω profile [integrated Fig. 8(a) from $\omega = -0.6^\circ$ to $\omega = 1.6^\circ$] shown in Fig. 8(c) remains nearly constant at the high field, while that at the zero-voltage region shows the slow fluctuation, up to a few milliseconds after the field change. The corresponding optical response in Fig. 8(c) shows the memory effect when the electric field is turned off ($+60 \rightarrow 0$ V, falling edge) and the sharp decrease when the field is turned on ($0 \rightarrow 60$ V, rising edge). Figures 9(a) and 9(b) show the detailed intensity variation at $\omega = 0^\circ$ and 0.4° at the falling edge and the rising edge, respectively. At the falling edge, the decrease of the ω -profile intensity depends on the ω angle, while at the rising edge the intensity increase seems to be independent of the ω angle. The transient time in the time-resolved ω profile, when it is defined by the time interval during which the ω intensity in Fig. 9 levels off after the electric field change, is ca. 0.2–0.4 ms for the falling edge and about 0.5 ms for the rising edge. The optical transient time is about $30 \mu\text{s}$ at the rising edge for this sample [Fig. 8(c)] and usually less than 0.1 ms; it is shorter than the layer transient time.

The time-resolved χ profiles for falling edge and rising edge are shown in Figs. 10(a) and 10(b), respectively. The time-resolved χ profiles have the double peak and the single peak at the high and the low voltage, respectively, and they correspond well to the quasistatic time-resolved χ profile shown in Fig. 7. The response time in the χ profile, during which the major profile change occurs after the applied field change, is 0.1–0.2 and 0.3–0.4 ms for the falling edge and the rising edge, respectively. The response time for the χ profile is slightly shorter than the transient time for the ω

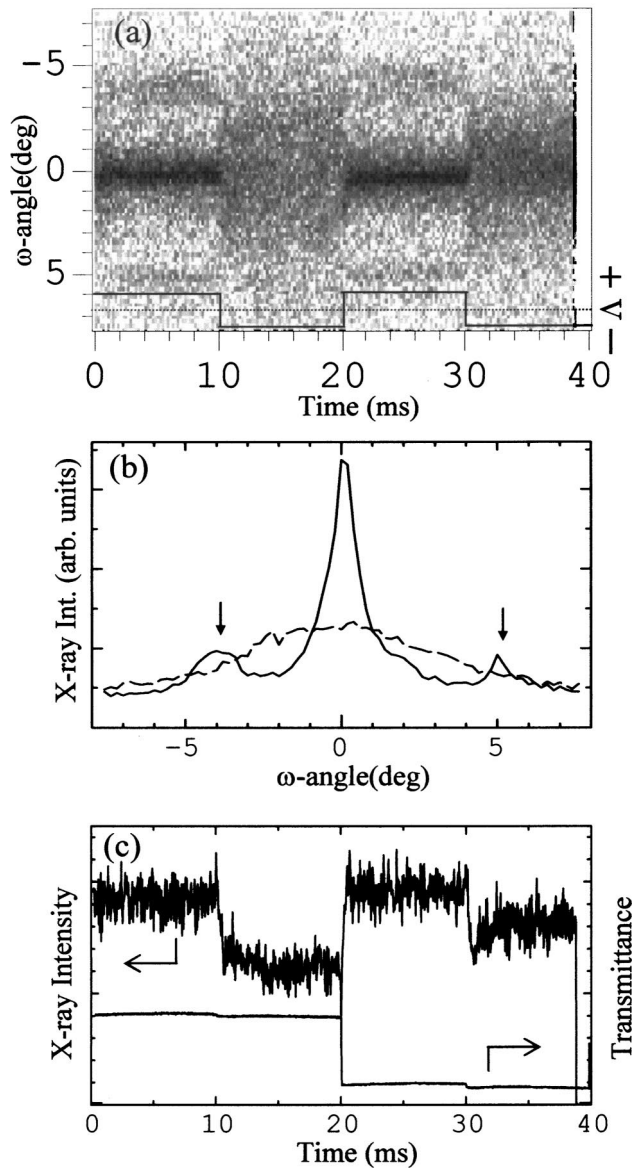


FIG. 8. (a) Time-resolved MCS-mode ω profiles for the step-form electric field (25 Hz, ± 60 V). 0.04 ms time resolution. An inset shows the wave form applied to the sample. (b) ω profiles integrated over 3 ms around 60 V (solid) and 0 V (broken). Arrows show humps that appeared at ± 60 V applied voltage. (c) The time dependence of the ω -profile integrated intensity around $\omega = 0.2^\circ - 1^\circ$ obtained from (a). An optical transmittance is also shown.

profile. This might be caused by the following reasons; the ω profile is the integrated intensity for the χ angle in the present experiment resulting in the insensitive response, and the marked change in the layer structure is closely related to the h chevron rather than the v chevron (or the layer deformation around the Y axis). In practice, the slow intensity variation in the χ profile (more than 1 ms) was observed and it corresponded to the slowly varying part of the ω profile.

D. AFLC response

An AFLC sample TFMHPOBC was also measured with the same technique. At the initial stage before the field ap-

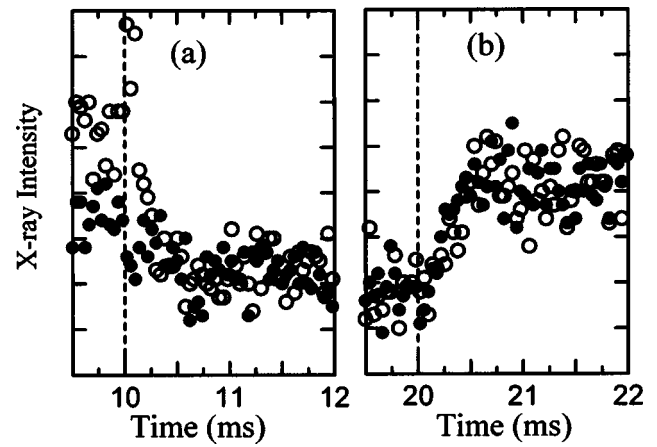


FIG. 9. X-ray intensity near the falling ($+60-0$ V) (a) and rising ($0-60$ V) (b) edges obtained from Fig. 8(a) for $\omega = 0^\circ$ (\circ) and $\omega = 0.4^\circ$ (\bullet). Dotted lines show the time when the applied field changes.

plication, the sample showed the stripe texture which was a combination of the v and the h chevron [28]. Figure 11 shows the applied voltage dependences of the angles δ and γ for TFMHPOBC together with those for TK-C101. A clear threshold voltage for TFMHPOBC (AFLC) in contrast to the gradual layer change in TK-C101 (FLC) agrees with previous experiments [9,17–19]. It is noted that not only δ but also γ shows the similar voltage dependence. The threshold voltage relates to the onset of the ferroelectric state.

During the reversible layer transformation under the triangular wave form (5 Hz, ± 65 V), the time-resolved MCS ω profile [Fig. 12(a)] shows the triple peak at the low field and the single peak at the high field. The corresponding time-resolved χ profile [Fig. 12(c)] shows that the two peaks at the high field (50 and 140 ms), though the low-angle peak (around $\chi \sim -1.5^\circ$) is quite weak in this case, become a

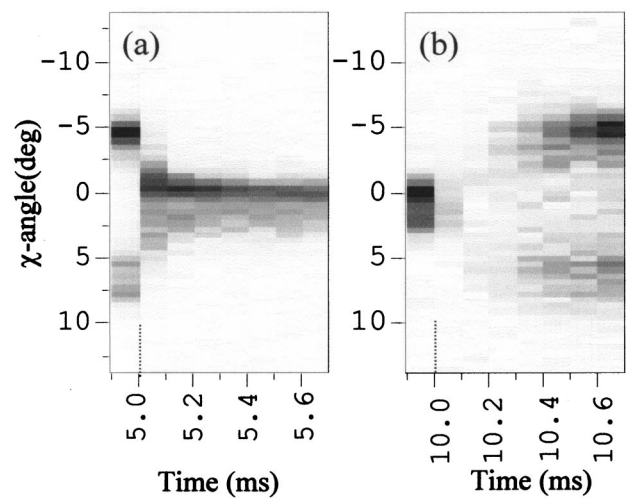


FIG. 10. (a) and (b) are time-resolved MCA-mode χ profiles for the falling edge ($+60-0$ V) and the rising edge ($0-60$ V), respectively, of the step-form electric field (50 Hz, ± 60 V); 0.1 ms time resolution. Dotted lines show the time when the applied field changes.

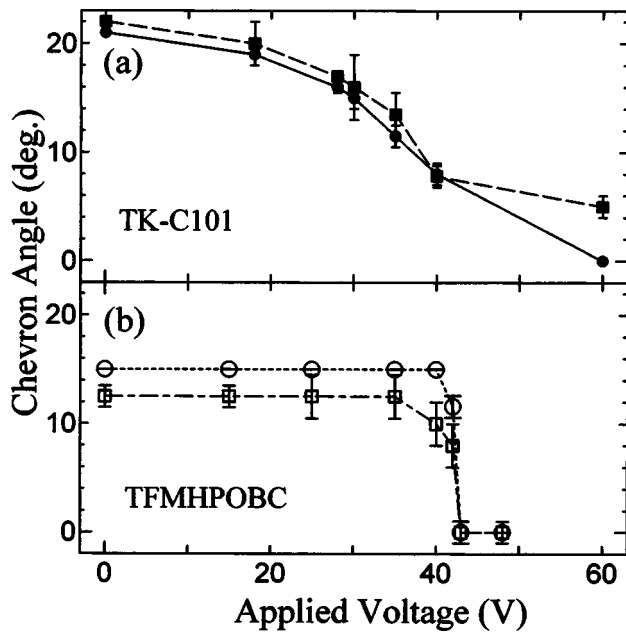


FIG. 11. Applied voltage dependences of the chevron angle δ (■,□) and γ (●,○). (a) and (b) are for TK-C101 (FLC) and TFMHPOBC (AFLC), respectively. The bar shows the FWHM of each peak.

single peak at the medium field (60, 80, and 130 ms) and that the two peaks appear again in the low field (90–110 ms). The angular separation between the two peaks at the low field is wider than that at the high field. From Figs. 12(a) and 12(c), the layer structure is approximately described as the h chevron at the high field, the quasibookshelf at the medium field, and the combination of the h and v chevrons at the low field. Compared to TK-C101 results and the similarity between the optical response and the diffraction intensity [Fig. 12(b)], it was confirmed that the layer structure of TFMHPOBC appearing in the high and medium fields corresponds to the ferroelectric state. The appearance of the low-field h chevron is closely related to the antiferroelectric state due to the field-induced phase transition. It is noted that the x-ray diffraction profile shows the double hysteresis similar to the optical response of AFLCs [2,9], indicating again the important role of layer motion in the electro-optical response.

The transient layer response under the step-form electric field (100 Hz, ± 45 V) shows the different behavior between the falling and rising edges. At the falling edge [Figs. 13(a) and 14(a) for ω and χ profiles, respectively], the ferroelectric structure gradually changes to the antiferroelectric one, while at the rising edge [Figs. 13(b) and 14(b)] the layer structure suddenly changes within a present time resolution. The transient time, during which the h chevron of the antiferroelectric and the ferroelectric phases for the falling (T_f) and rising (T_r) edges, respectively, appears after the field change, depends on the sample. Typically, T_f and T_r were 0.1–0.3 and 0.02–0.08 ms, respectively, and corresponded to the slow component of the field-induced phase transition [30]. The quick response of T_r is closely related to the field-induced phase transition. The layer transient time was as fast as the optical response time.

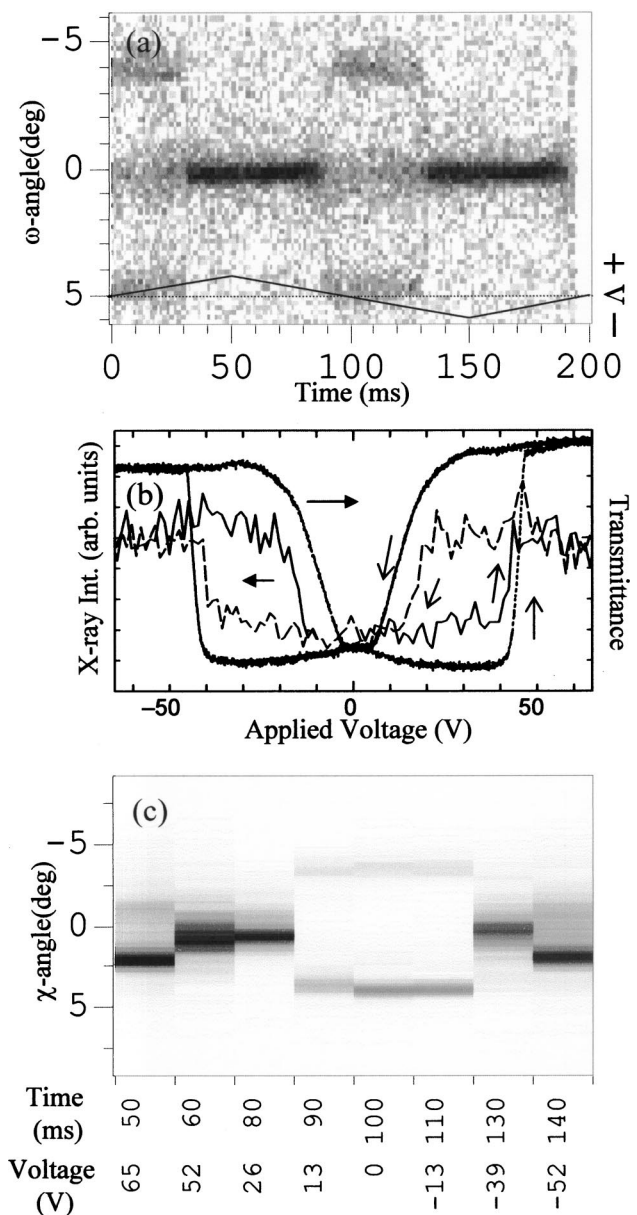


FIG. 12. (a) Time-resolved MCS-mode ω profiles for one cycle of the triangular wave form (5 Hz, ± 65 V) for TFMHPOBC. The applied wave form is shown in an inset. 0.5 ms time resolution. (b) The applied voltage dependence of the ω -profile intensity near $\omega=0^\circ$ (voltage-dependence profile) from (a). The optical transmittance is also shown. (c) Time-resolved MCA-mode χ profiles obtained at $\omega=+0.2^\circ$. 5 ms time resolution. The time from 50 to 150 ms corresponds to the applied voltage from +65 to -65 V. Note that the sampling time (abscissa) is not equal interval. The sample thickness was 5.5 μm .

IV. DISCUSSION

A. Layer structure under the electric field

Since a series of spatially and time-resolved ω - and χ -diffraction profiles was measured, the irreversible and reversible layer transformations of the surface-stabilized FLCs under the electric field can be discussed as shown in Fig. 15.

At the initial state, the layer structure is the v chevron with a zigzag defect [Fig. 15(a)]. The irreversible layer trans-

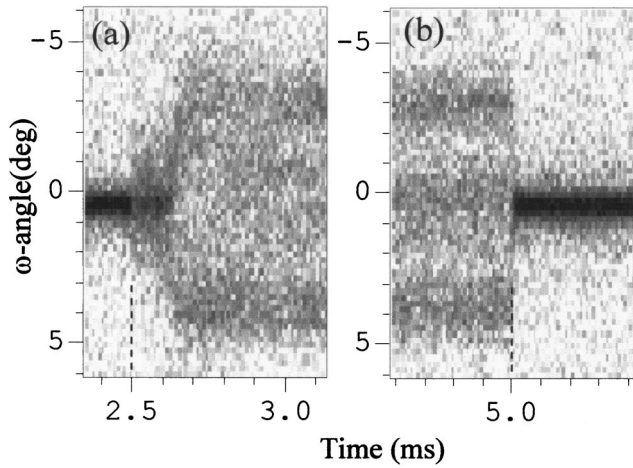


FIG. 13. Time-resolved MCS-mode ω profiles for the step-form electric field (100 Hz, ± 45 V) from TFMHPOBC around the falling edge (+45–0 V) (a) and the rising edge (0–45 V) (b). 10 μ s time resolution. Dotted lines show the time when the applied field changes. The sample thickness was about 4 μ m.

formation with increasing electric field consists of two stages. When the electric field is first applied to the sample, the electric torque makes the layer upright resulting in the needle-defect generation [Fig. 15(b)]. The in-plane deflection angle γ is nearly equal to the v-chevron angle δ at this stage, though the layer bends along the depth. With an increasing applied voltage, the nearly periodic structure consisting of the alternate v chevron and h chevron is achieved [Fig. 15(c)]. These structures are deduced from the data shown in Figs. 3(1-a,b) and 3(2-a,b) and each layer structure has already been discussed [12,21,22].

With further increase of the applied voltage, both δ and γ reduce gradually and simultaneously. There are, at least, two

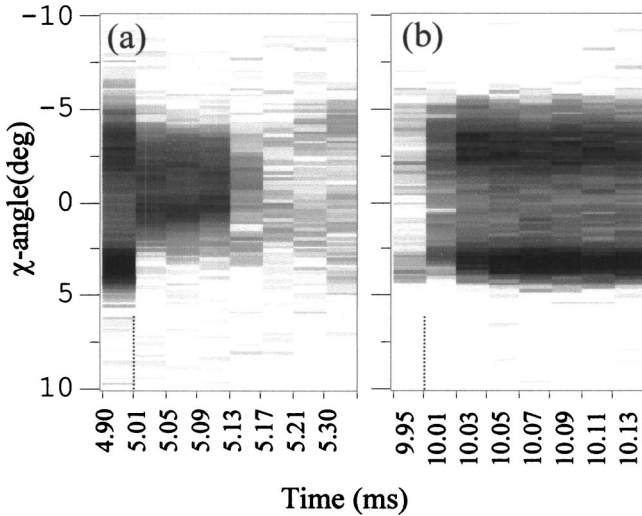


FIG. 14. Time-resolved MCA-mode χ profiles for the step-form electric field (50 Hz, ± 45 V) from TFMHPOBC for the falling edge (+45–0 V) (a) and the rising edge (0–45 V) (b). 40 and 15 μ s time resolutions for (a) and (b), respectively. Dotted lines show the time when the applied field changes. Note that the sampling time (abscissa) is not equal interval.

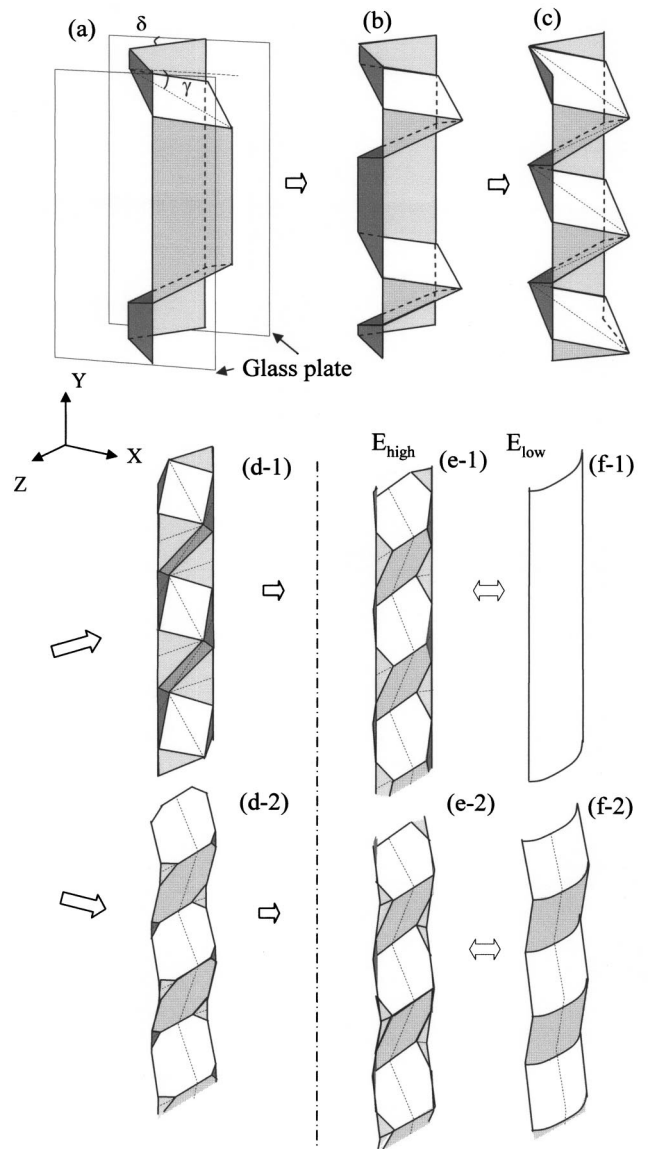


FIG. 15. Schematic representation of the local-layer structure in the FLC cell under the ac electric field. The initial v-chevron structure with narrow walls (a), the generation of the needle defect (b), the development of the needle defect and the formation of the stripe texture (c), and the transformation of the stripe texture (d). The reversible layer transformations are shown in (e) and (f) for the high (E_{high}) and low (E_{low}) electric fields, respectively. (d-1)–(f-1) and (d-2)–(f-2) correspond to the type *S* and type *D* layer transformations (see text). All chevron angles are exaggerated and the layer deformation, especially along the depth, is simplified. Thin dotted lines are a guide for eyes to show the folding direction.

types of the surface layer structure: either the layer intersection at the substrate surface is straight [type *S*, Fig. 15(b-1)] or a part of the surface layer is folded [type *D*, Fig. 15(b-2)]. The surface layer of the type *D* has partly changed to the h chevron. The type *S* structure is deduced from Fig. 4, in which the quite broad bookshelf or the deformed v-chevron structure is realized without the h chevron after turning off the field. The single peak at the low voltage in a reversible process in Fig. 7(b) also supports this structure. The type *D*

layer structure is inferred from Figs. 3(5-a) and 3(5-b) by considering that the h-chevron area increases to make up the decrease in the v-chevron part. The origin of types *S* and *D* might be due to the difference in the surface treatment and/or the history of the applied field.

The quasistatic reversible layer deformation is illustrated in Figs. 15(e) and 15(f) for the high and low fields, respectively (see Figs. 6 and 7). When the quasibookshelf is realized at the low field (type *S*), the layer bends along the cell depth [Fig. 15(f-1)]. With increasing field, the bulk layer tends to be upright while the surface layer stays almost at the same position, resulting in the appearance of the surface v chevron at the apex of the h chevron, which enables the smooth layer connection [Fig. 15(e-1)]. The v-chevron part corresponds to the small hump appeared in the time-resolved ω profile. When the layer is the deformed h chevron even at the low field (type *D*), the layer response to the electric field is the increase in the h-chevron angle and the appearance of the weak v-chevron component at the high field [Fig. 15(e-2)]. The present results directly show the importance of the substrate surface effect during the h-chevron formation.

After the electric field is turned off, the type *S* structure becomes the broad quasibookshelf or the strongly modified v chevron as seen in Figs. 4(c) and 4(d). For the type *D* structure, the layer is similar to the mostly h-chevron structure shown in Fig. 15(b-2) but with the distortion along the depth.

In Fig. 15, the layer is assumed to be symmetric with respect to the center of the cell for simplicity. In practice, however, the layer might be asymmetric due to the difference in the surface treatment, macroscopically and microscopically, for upper and lower substrates.

B. Origins of the layer deformation

The possible origin of the observed layer deformation is discussed in terms of the electric torque, the substrate surface anchoring, and the molecular orientation. In the following discussion, the conservation of the layer spacing is assumed.

1. Stripe texture formation under electric field

For the generation and the growth of the needle defect, the surface molecule is not necessary to change orientation. Thus, the needle defect is easy to grow [12,24]. With increasing electric field, the angles δ and γ became small simultaneously [Fig. 15(d)] in contrast to the proposed layer structure in which the h chevron grows continuously with increasing applied voltage [12]. The layer spacing along the rubbing direction at the substrate surface ds is given by $ds = dc^*/\cos \delta \cos \gamma$, where $dc^* = da \cos \theta$ is the smectic layer spacing, da is the molecular length, and θ is the cone angle. At the initial and low-field stages, the angles δ and γ are close to θ indicating $ds \sim da$. The decrease in both δ and γ is the clear and direct evidence of the rearrangement of the surface molecule; thus ds reduces. This process is induced by the increasing field-induced torque, which overcomes the surface anchoring. The competition between the electric torque and the surface anchoring induces a strain in the bulk resulting in the appearance of dense focal conics [Fig. 2(c)]. After the new layer structure forms at higher voltages, focal

conics disappear. It is noted, however, that the surface molecule does not completely follow the applied field due to the resistive anchoring. Thus the perfect bookshelf structure is seldom observed. Furthermore, surface molecules arrange again after a long interval so that they can become parallel to the rubbing direction slowly (uppermost figure of Fig. 5). Various types of so-called stripe textures are observed after the generation of the needle defect; the layer structure, however, is different among them. The triple peak in the ω profile for the stripe texture obtained with conventional x-ray experiments has been interpreted as the v chevron with the bookshelf at the center of the cell (double-kink structure) [9,17,19]. From the present results, the bookshelf region might be interpreted as a part of the h chevron [Fig. 15(d)] in some cases.

2. Layer structure in the reversible transformation

During the reversible layer transformation process, the layer at the surface is assumed to stay almost at the same position due to the surface anchoring, while the bulk layer (molecule) responds to the applied field under this boundary condition. At the low field, the so-called quasibookshelf structure seems to be realized [Figs. 6, 7, and 15(f)]. The low-field structure, however, is expected to be the v chevron, if constant dc^* is assumed, since the high electric field structure is mainly the h chevron [Fig. 15(e)]. Furthermore, even after turning off the field, the perfect v chevron as seen in the initial state was not observed. The layer structure at the low field is explained as follows. Since the homogeneously bent layer is energetically unfavorable in the smectic phase, the broad peak in the ω profile indicates the introduction of the layer imperfection; i.e., the alignment condition is partly destroyed by the high-field treatment. In other words, as is well known, the good alignment is necessary to realize the v chevron. Even when the macroscopic alignment condition is deteriorated, however, the v chevron may be locally realized at least near the surface to keep the layer spacing constant. From these discussions, the quasibookshelf structure observed at the low field seems to be the imperfect v-chevron structure.

The electric torque makes the layer upright resulting in the h-chevron formation at the high field, whereas the surface anchoring tends to align the v-chevron layer. The difference in the transient layer response between the falling and rising edges observed in Figs. 9 and 10 can be explained by these two forces. At the rising edge, the molecule should overcome the surface anchoring, while the anchoring force alone exists at the falling edge. Thus, in the FLCs, the transient time at the rising edge is slower than that at the falling edge.

Under both triangular- and step-form electric fields, the layer transformed depending on the electric field, while the optical response showed the well-known memory effect [Figs. 6(c) and 8(c)]. In other words, the bulk molecular position moves while the molecular orientation remains nearly the same during the layer deformation. The time-resolved diffraction measurement clarified the molecular motion that was not observed by the optical measurement alone.

V. CONCLUSION

The time-resolved x-ray microdiffraction measurement clarified the local-layer structure response in FLC cells to the electric field. The temporally and spatially resolved ω and χ profiles can offer the information for the reconstruction of the time dependent layer structure, which has been estimated from indirect observations. The initial v-chevron structure changed to the combination of the v chevron and the h chevron at relatively low electric field as the growth of the needle defect. The chevron angles then reduced continuously with increasing electric field. After the irreversible layer transformation, the transition between the h chevron with a small v-chevron part (high field) and the so-called quasibookshelf (low field) occurred reversibly during the ac field application. The low-field quasibookshelf seems to be the imperfect v-chevron structure. The electric torque and the surface anchoring are major driving forces for the reversible layer transformation. Time-resolved measurements also revealed the difference in the response between the local layer and the molecular orientation. The reversible transformation process in the FLC cell corresponds well to that in the ferroelectric state of the AFLC cell.

Further studies of the static and dynamic details of the h-chevron structure and its relation to the v chevron are necessary to reveal the mechanism of the stripe texture formation and to study the role of the layer ordering in the electro-optical response. The effects of the polarity and the asymmetry of the electric field on the layer stability are also of practical interest. Further experiments are now underway to clarify these problems.

ACKNOWLEDGMENTS

The authors would like to thank the staff of PF for their help during experiments. We wish to thank Professor K. Sekizawa, Professor Y. Takano, and Dr. K. Takase for their continuous encouragement during the study. This work was carried out under the approval of the Photon Factory Program Advisory Committee (Proposal Nos. 98G341 and 00G279). This work was partly supported by a Grant-In-Aid for Scientific Research on Priority Area (B) (Grant Nos. 2129202 and 12129206), the Ministry of Education, Science, Sports and Culture.

-
- [1] N. A. Clark and S. T. Lagerwall, *Appl. Phys. Lett.* **36**, 899 (1980).
 - [2] S. T. Lagerwall, *Ferroelectric and Antiferroelectric Liquid Crystals* (Wiley, Weinheim, 1999).
 - [3] T. P. Rieker, N. A. Clark, G. S. S. Smith, D. S. Parmar, E. B. Sirota, and C. R. Safinya, *Phys. Rev. Lett.* **59**, 2658 (1987).
 - [4] N. Clark and T. P. Rieker, *Phys. Rev. A* **37**, 1053 (1988).
 - [5] N. A. Clark, T. P. Rieker, and J. E. MacLennan, *Ferroelectrics* **85**, 79 (1988).
 - [6] Y. Ouchi, H. Takano, H. Takezoe, and A. Fukuda, *Jpn. J. Appl. Phys., Part 1* **27**, 1 (1988).
 - [7] H. Orihara, A. Suzuki, Y. Ishibashi, K. Gouhara, Y. Yamada, and N. Yamamoto, *Jpn. J. Appl. Phys., Part 2* **28**, L676 (1989).
 - [8] Y. Sato, T. Tanaka, H. Kobayashi, K. Aoki, H. Watanabe, H. Takeshita, Y. Ouchi, H. Takezoe, and A. Fukuda, *Jpn. J. Appl. Phys., Part 2* **28**, L483 (1989).
 - [9] M. Johno, Y. Ouchi, H. Takezoe, A. Fukuda, K. Terashima, and K. Furukawa, *Jpn. J. Appl. Phys., Part 2* **29**, L111 (1990).
 - [10] K. Itoh, M. Johno, Y. Takanishi, Y. Ouchi, H. Takezoe, and A. Fukuda, *Jpn. J. Appl. Phys., Part 1* **30**, 735 (1991).
 - [11] M. Oh-e, M. Isogai, and T. Kitamura, *Liq. Cryst.* **11**, 101 (1992).
 - [12] R. F. Shao, P. C. Willis, and N. A. Clark, *Ferroelectrics* **121**, 127 (1991).
 - [13] Y. Asao and T. Uchida, *Jpn. J. Appl. Phys., Part 2* **32**, L604 (1993).
 - [14] A. G. Rappaport, P. A. Williams, B. N. Thomas, N. A. Clark, M. B. Ros, and D. M. Walba, *Appl. Phys. Lett.* **67**, 362 (1995).
 - [15] R. E. Geer, S. J. Singer, J. V. Selinger, B. R. Ratna, and R. Shashindhar, *Phys. Rev. E* **57**, 3059 (1998).
 - [16] L. S. Matkin, H. F. Gleeson, L. J. Baylils, S. J. Watson, N. Bowring, A. Seed, M. Hird, and J. W. Goodby, *Appl. Phys. Lett.* **77**, 340 (2000).
 - [17] S. J. Watson, L. S. Matkin, L. J. Baylis, N. Bowring, H. F. Gleeson, M. Hird, and J. Goodby, *Phys. Rev. E* **65**, 031705 (2002).
 - [18] P. Cluzeau, P. Barois, H. T. Nguyen, and C. Destrade, *Eur. Phys. J. B* **3**, 73 (1998).
 - [19] P. Cluzeau, P. Barois, and H. T. Nguyen, *Eur. Phys. J. E* **7**, 23 (2002).
 - [20] A. Iida, T. Noma, and H. Miyata, *Jpn. J. Appl. Phys., Part 1* **35**, 160 (1996).
 - [21] A. Iida, T. Noma, and H. Miyata, *Jpn. J. Appl. Phys., Part 1* **38**, 2845 (1999).
 - [22] A. Iida, T. Noma, and H. Miyata, *Jpn. J. Appl. Phys., Part 1* **40**, 1345 (2000).
 - [23] Y. Takanishi, A. Iida, K. Ishikawa, H. Takezoe, and A. Fukuda, *Jpn. J. Appl. Phys., Part 1* **35**, 683 (1996).
 - [24] Y. Takanishi, A. Iida, K. Ishikawa, H. Takezoe, and A. Fukuda, *Jpn. J. Appl. Phys., Part 1* **38**, 4132 (1999).
 - [25] Y. Takanishi, T. Izumi, J. Watanabe, K. Ishikawa, H. Takezoe, and A. Iida, *J. Mater. Chem.* **9**, 2771 (1999).
 - [26] H. Gleeson and A. Mors, *Liq. Cryst.* **21**, 755 (1996).
 - [27] H. Gleeson, G. Bryant, and A. Morse, *Mol. Cryst. Liq. Cryst.* **362**, 203 (2001).
 - [28] Y. Takahashi, A. Iida, Y. Takanishi, T. Ogasawara, K. Ishikawa, and H. Takezoe, *Jpn. J. Appl. Phys., Part 1* **40**, 3294 (2000).
 - [29] Y. Takahashi, A. Iida, Y. Takanishi, T. Ogasawara, K. Ishikawa, and H. Takezoe, *Mol. Cryst. Liq. Cryst.* **365**, 853 (2001).
 - [30] M. Johno, K. Ito, J. Lee, Y. Ouchi, H. Takezoe, A. Fukuda, and T. Kitazume, *Jpn. J. Appl. Phys., Part 2* **29**, L107 (1990).

Temperature and Electric Field Dependences of the Local Layer Structure in Anti-Ferroelectric Liquid Crystals Measured by X-Ray Micro-Diffraction

YUMIKO TAKAHASHI,¹ ATSUO IIDA,² YOICHI TAKANISHI,³
MICHI NAKATA,³ KEN ISHIKAWA,³ and HIDEO TAKEZOE³

¹*Department of Physics, College of Science and Technology, Nihon University, 1-8, Surugadai, Kanda, Chiyoda-ku, Tokyo 101-8308, Japan*

²*Photon Factory, Institute of Materials Structure Science, High Energy Accelerator Research Organization, 1-1 Oho Tsukuba 305-0801, Japan*

³*Department of Organic and Polymeric Materials, Tokyo Institute of Technology, O-okayama, Meguro-ku, Tokyo 152-8552, Japan*

(Received in final form October 29, 2003)

The local layer of the antiferroelectric liquid crystal has been investigated as a function of the temperature near the SmA to SmC_A^{} phase transition by synchrotron X-ray microbeam diffraction. The stripe texture in the SmA phase well above the phase transition temperature is related to the in-plane layer deflection. Just above the phase transition temperature, the clear stripe starts to grow and the local layer structure becomes the combination of the vertical-chevron and the horizontal-chevron. With decreasing temperature in the SmC_A^{*} phase, the chevron angle increases. The growth of the chevron structure is explained by the gradual reduction of the layer spacing. The time resolved measurement of the local layer structure in the electroclinic effect is also carried out to characterize the layer response in the SmA phase. The comparison of the chevron structure between the antiferroelectric and the ferroelectric liquid crystal is made.*

Keywords Anti-ferroelectric liquid crystal; stripe texture; chevron local layer structure; electroclinic; synchrotron X-ray microbeam; X-ray micro-diffraction

1. Introduction

Antiferroelectric liquid crystals (AFLCs) have been attracted much attention for their tristable switching behavior and various sub-phases [1, 2] from both basic and applied researches. Smectic sub-phases and the phase transition between them in AFLCs related closely to the molecular arrangement in adjacent smectic layers. The layer structure characterizes also the smectic sub-phase, as it reflects the molecular interaction mainly through the layer spacing and the surface effect for the surface stabilized (SS) AFLC. For instance, the bookshelf layer structure is realized in the SS cell in the smectic A phase (SmA), while the vertical chevron layer structure (v-chevron) is generated in smectic C^{*} (SmC^{*}) variants due to the layer spacing reduction. Furthermore, a stripe texture running parallel to the rubbing direction is sometimes observed with a polarized optical microscope in AFLC and the ferroelectric liquid crystal (FLC) [3] and is thought to be due to the horizontal chevron (h-chevron, in-plane chevron.). To clarify the relation between these local layer

structures and the molecular alignment, small angle X-ray scattering investigations [4–7] have been carried out. Recently the time resolved synchrotron X-ray microbeam has been successfully applied to the AFLC and FLC [8–10] to reveal the dynamic response of the spatially resolved local layer structure under the electric field.

In this paper, in order to directly characterize the stripe texture and to investigate its growth process, the temperature dependence of the local layer structure was measured in detail using synchrotron X-ray microbeam diffraction. The time resolved X-ray diffraction measurement of the electroclinic effect is also carried out to characterize the layer response in the SmA phase. The chevron structure in AFLC is compared with that in FLC.

2. Experimental

The experiment was carried out on BL-4A at the Photon Factory. The X-ray energy was 8 keV and the beam size at the sample was less than $3(\text{vertical}) \times 4(\text{horizontal}) \mu\text{m}^2$. The diffracted intensities were measured as a function of angles ω and χ , which correspond to the layer orientation with respect to the rubbing direction normal in the cell plane and the surface normal, respectively. The layer deflection angles, δ and γ , are measured from the ideal bookshelf structure along the depth and in the cell glass plane, respectively. When the v- or h-chevron structure is realized, δ or γ is equivalent to the chevron angle. The sample geometry is shown in Fig. 1. Diffracted X-rays were measured by a position sensitive proportional counter or an X-ray CCD detector with an image intensifier. The time resolved measurements were performed by using a timing control system synchronized with an applied signal to the sample. A detailed description of the experimental system has been already published elsewhere [8–10].

The samples were homogeneously aligned (R)-TFMHPOBC (AFLC) and was sandwiched between ITO-coated glass plate ($150 \mu\text{m}$ thick) rubbed on one-side after coating a polyimide alignment film. The cell gap was about $9 \mu\text{m}$. The sample was set in a conventional temperature control stage. The rubbing direction was set horizontally. The phase transition temperature (T_c) from SmA to SmC_A^{*} was 109°C [11]. Several samples were prepared for different experiments to confirm the effect of the thermal history or electric field treatment.

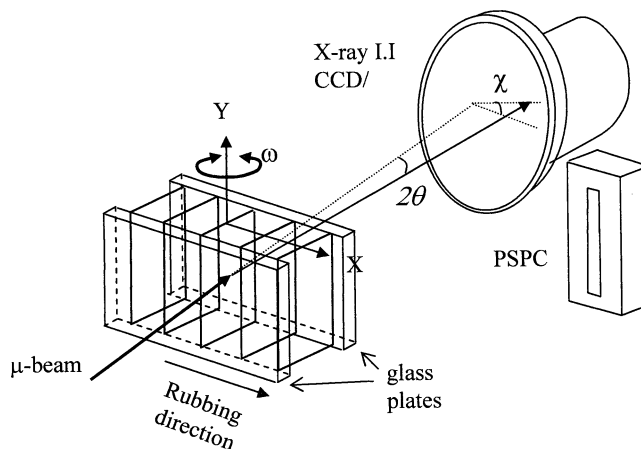


FIGURE 1 Schematic representation of the experimental setup for the synchrotron X-ray microbeam diffraction.

3. Results

The spatial distribution of the X-ray diffraction profile from TFMHPOBC was measured as a function of temperature near the SmA to SmC_A* phase transition together with the *in situ* observation of the texture by a polarized optical microscope.

At $T_c + 2.9^\circ\text{C}$, the micrograph (Fig. 2(a)) shows the stripe texture of a weak contrast. Figures 3(a) and (b) show series of ω - and χ -profiles, respectively, scanned in the vertical direction normal to the stripe texture. Both profiles show single peaks almost independent of the position. The fluctuation of the peak angular position are within $\pm 1^\circ$. Above this temperature, at least up to $T_c + 7^\circ\text{C}$, ω - and χ -profiles are almost unchanged. By decreasing the temperature, at $T_c + 1.9^\circ\text{C}$, the full width at half maxima (fwhm) of the peak in the spatially resolved ω -profiles increases from 1.1° (Fig. 3(a)) to 1.7° (Fig. 3(c)) on average and the tail part of the profile is enhanced. The peak angular position in the χ -profile in Fig. 3(d) shows the slightly larger angular fluctuation than that in Fig. 3(b). The contrast of the stripe texture (Fig. 2(b)) slightly increases compared to Fig. 2(a). At $T_c + 1^\circ$, in the ω -profile (Fig. 3(e)), the single or the triple peak (a strong central peak and two weak sub-peaks) appears alternately from position to position. The angular position of the sub-peak is about 2° from the main peak. At the same time, the angular position of the peak in the χ -profile (Fig. 3(f)) shows the alternate intensity distribution; its spatial period is about

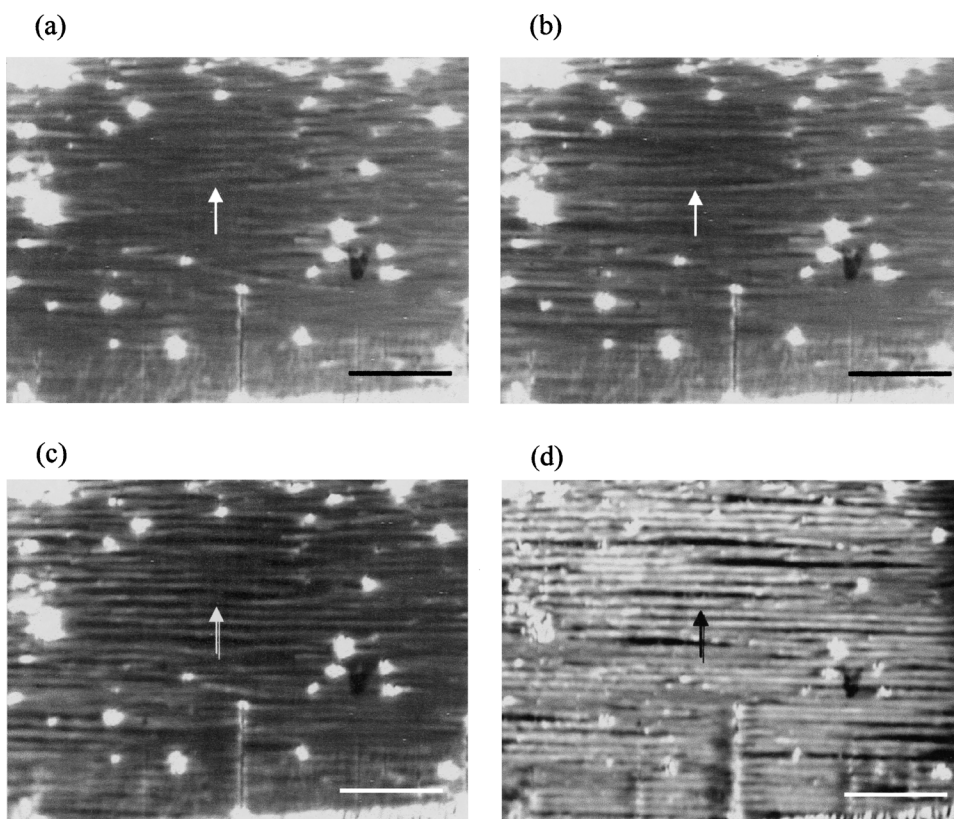


FIGURE 2 Polarized optical micrographs of textures obtained at temperatures (a) $T_c + 2.9^\circ$, (b) $T_c + 1.9^\circ$, (c) $T_c + 1.0^\circ$ and (d) $T_c - 1.0^\circ$. The rubbing direction was set horizontally. White arrows show the direction and the region of the X-ray measurement shown in Fig. 3. A scale mark is $100\ \mu\text{m}$.

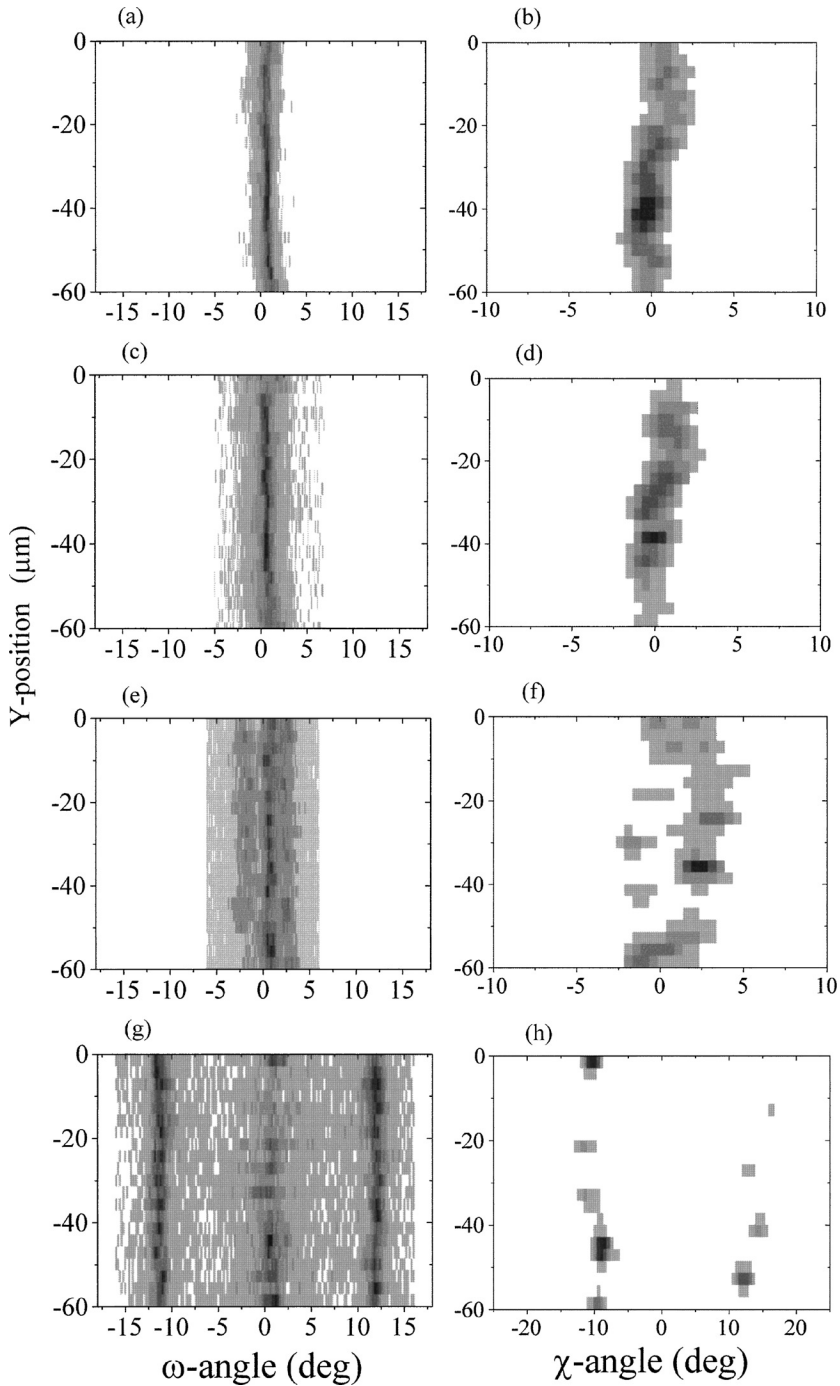


FIGURE 3 Series of ω -profiles and χ -profiles as a function of the vertical position (Y-direction) at $T = T_c + 2.9^\circ$, (a) and (b), $T = T_c + 1.9^\circ$ (c) and (d), $T = T_c + 1.0^\circ$ (e) and (f), and $T = T_c - 1.0^\circ$ (g) and (h). The χ -profiles were obtained at $\omega = 0.6^\circ$ (b), 0.5° (d), 0.8° (f) and 0.8° (h). The scanning step in the Y direction was $3 \mu\text{m}$. The darker part corresponds to the higher diffracted intensity. X-ray intensities were normalized by the highest intensity in each figure.

10 μm and the angular difference of the alternate peak position is about $4\text{--}5^\circ$. When the sample is further cooled down to SmC_A^* , $T_c - 1^\circ\text{C}$ (Fig. 2(d)), the triple peak is clearly observed in the ω -profile (Fig. 3(g)). The peak intensity for the main ($\omega = 0^\circ$) and sub-peaks ($\omega = \pm 12^\circ$) varies alternately again as a function of the position. The corresponding χ -profile (Fig. 3(h)) also shows the alternate peaks.

Figure 4 shows the peak angular position in the χ -profile at around $\omega = 0.8^\circ$, $\omega = -11.2^\circ$ and $\omega = 12.0^\circ$ at $T_c - 1^\circ$. The peak of the χ -profile at $\omega = 0.8^\circ$ shows the nearly periodic variation, while those at $\omega = -11.2^\circ$ and $\omega = 12.0^\circ$ stay constant. The former and the latter are the typical behavior of the h- and v-chevron, respectively. Furthermore, the alternate appearance of each chevron structures indicates that the local layer structure is the combination of the h- and v-chevron; i.e. the periodic v-chevron and h-chevron structure is clearly generated at this temperature. The v- and h-chevron angles increased up to 15° at $T_c - 10^\circ\text{C}$.

Corresponding to these X-ray diffraction results, the stripe texture in Fig. 2 progressively increases its contrast. Though the stripe texture at high-temperature (Fig. 2(a)) is similar to that at low-temperature (Fig. 2(d)) except the contrast, the fine structure or the absolute position of the stripe is slightly different between them. The stripe seems to be modified near the defect (white dots in micrographs) around T_c .

The temperature dependence of the layer spacing was also measured with an X-ray CCD camera. The relative layer spacing as a function of temperature (Fig. 5(b)) was obtained from the diffraction spot on the CCD (Fig. 5(a)). T_c in this figure is set at the temperature where the layer spacing changes abruptly. Naturally, the layer spacing decreases rapidly in SmC_A^* with decreasing temperature due to the increase in the molecular tilt angle, it is also noted that the layer spacing gradually decreases even above T_c . This type of the temperature dependence has been also reported in other AFLC materials such as MHPOBC [12].

From the above experiment, it is clarified that the local layer in the SmA is approximately the so-called bookshelf structure and becomes the chevron structure near T_c . In order to characterize the local layer structure in further detail, the layer response to the electric fields (the electroclinic effect) was measured. Figures 6(a) and (b) show series of ω - and χ -profiles, respectively, scanned in the vertical direction normal to the stripe texture at $T_c + 1.0^\circ\text{C}$ without the electric field. The sample was different from that used in Fig. 3. Though a lot of defects and domains are seen in an optical micrograph (Fig. 7(a)), the measured region was in a single domain owing to the small beam size. In this sample, the v-chevron structure is not so clear (Fig. 6(a)) compared to that in Fig. 3(e), while

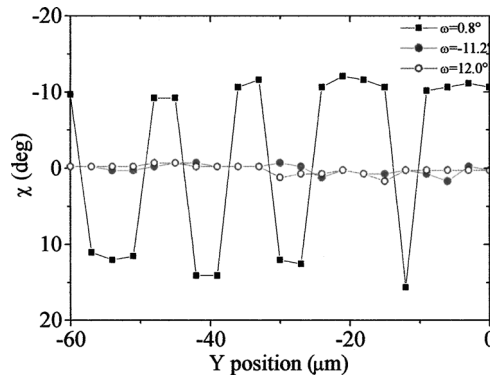


FIGURE 4 The peak angular position of the χ -profile (Fig. 3(h)) at around $\omega = 0.8^\circ$ (■), $\omega = -11.2^\circ$ (●) and $\omega = 12.0^\circ$ (○) at $T_c - 1^\circ$.

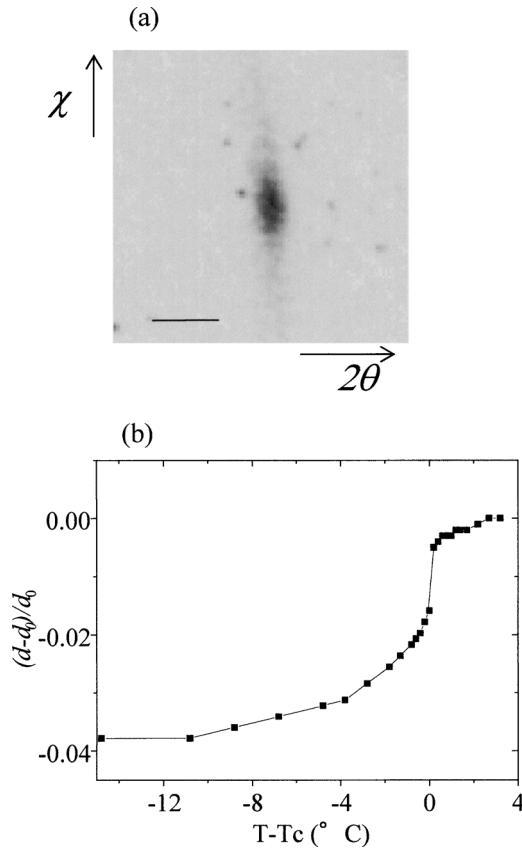


FIGURE 5 (a) X-ray diffraction spot obtained by an X-ray CCD camera at $T_c - 1^\circ$ at $\omega = -11.2^\circ$. A scale mark shows 0.1° in 2θ angle. (b) The relative layer spacing as a function of temperature. The T_c was set at the temperature where the gradient of the layer spacing has maximum. The layer spacing in SmA (d_0) is assumed to be 34.6 Å in this figure.

the h-chevron is partly realized (Fig. 6(b)). After the application of the triangular electric field (± 60 V, 5 Hz), the angular spread of the ω -profile becomes narrow (Fig. 6(c)). The time resolved ω -profile (Fig. 8(a)), though quite weak in the intensity, shows that the peak becomes broad and narrow at the low and high field, respectively. The narrow ω -profile in Fig. 6(c) is mainly due to the high field layer structure. The time-resolved χ -profile shows the single peak at the low field and the double peak at the high field (Fig. 8(b)). The positional dependence of χ -profile at the highest voltage are shown in Fig. 6(d). The h-chevron formation is clearly seen at the high field. Though the alternate change of the peak angular position is similar to that in Fig. 6(b), the angular separation of the low and high angle peaks becomes large. From this figure, it is found that the electroclinic effect results in the h-chevron formation which is characterized by the enhancement of the initial layer undulation. When the applied field is turned off, the local layer structure returns to the structure similar to the initial one (Figs. 6(e) and (f)). Furthermore, when the sample is cooled down to $T_c - 10^\circ\text{C}$ after the electric field treatment (Figs. 6(g) and (h)), the layer structure becomes again the combination of the v-chevron and the h-chevron. The position of the h-chevron and the fine structure, however, are slightly different from the initial ones, indicating the rearrangement of the layer structure.

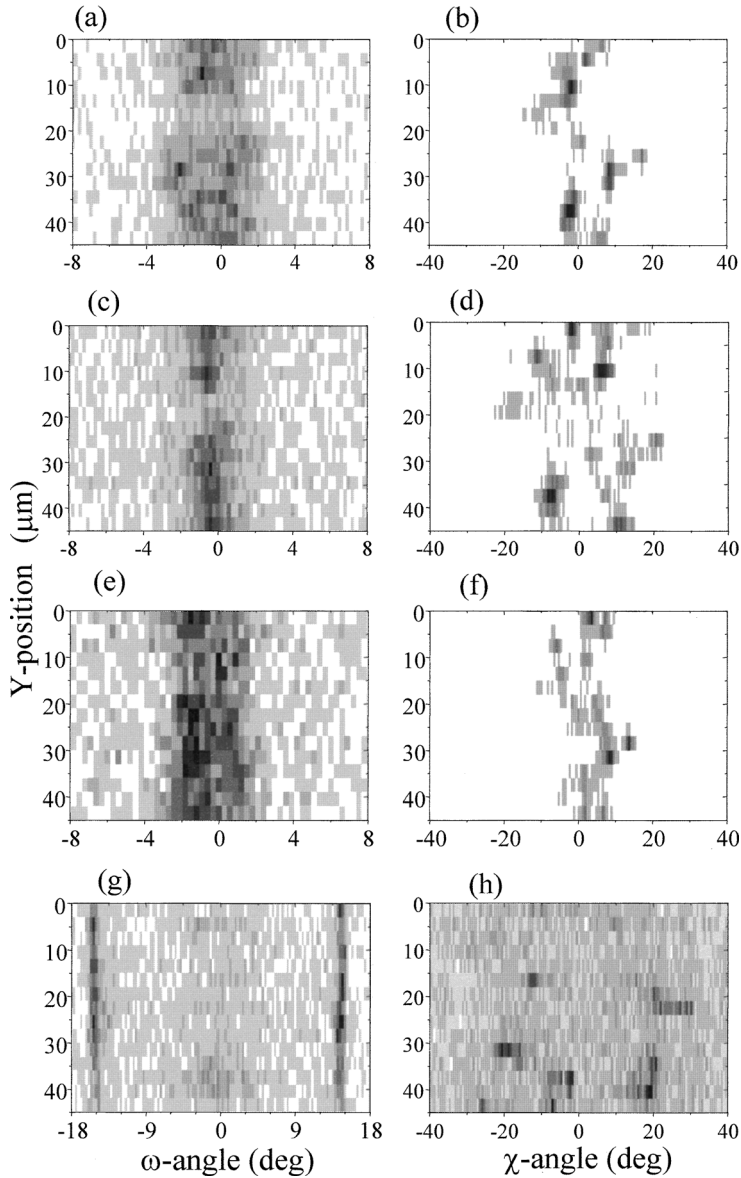


FIGURE 6 Series of ω -profiles and χ -profiles as a function of the vertical position (Y-direction) at $T_c + 1^\circ\text{C}$ before, (a) and (b), during, (c) and (d), and after, (e) and (f), the triangular electric field application (± 60 V, 5 Hz). (g) and (h) were obtained at $T_c - 10^\circ\text{C}$. (c) is a time integrated ω -profile, while (d) is a time resolved χ -profile at the high field. The χ -profiles (b), (d), (f) and (h) were obtained for $\omega = -1.8^\circ$, -0.6° , -1.5° and $\omega = 0^\circ$, respectively. The scanning step in the Y direction was $3\ \mu\text{m}$.

4. Discussion

The stripe texture in SmA of a relatively weak contrast is related to the local layer undulation observed in the χ -profile (Figs. 3(b)), which mainly consists of the in-plane layer deflection. With decreasing temperature, the fwhm of the ω -profile (Fig. 3(c)) gradually increases and the in-plane undulation structure grows (Fig. 3(d)). Just above $T_c(T_c + 1^\circ$.

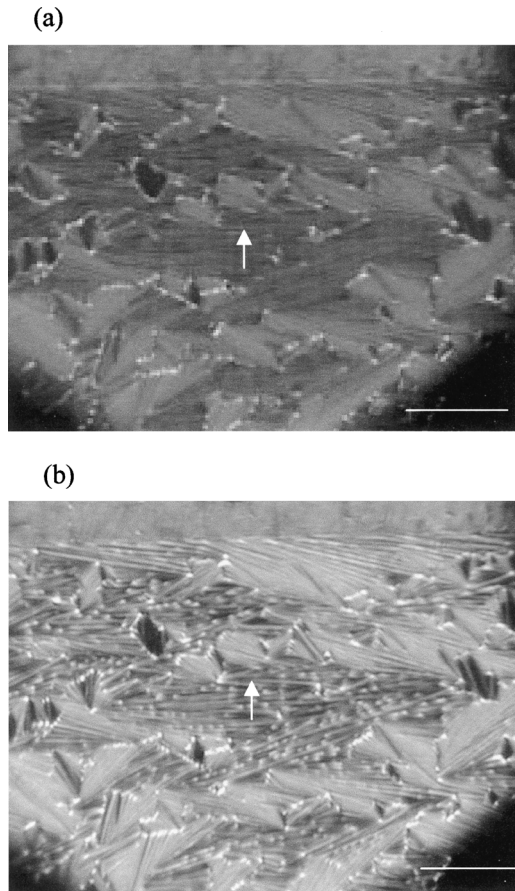


FIGURE 7 Polarized optical micrographs of the sample obtained during the electric field application at $T_c + 1.0^\circ$ (a) and after turning off the field at $T_c - 10^\circ$ (b). The spacer edge is shown in the upper part of the figure.

Figures 3(e) and (f), the v-chevron and the h-chevron (periodic in-plane deflection layer) appear simultaneously. The temperature dependence of the layer structure is considered to be due to the reduction of the layer spacing (Fig. 5(b)) in the same way as the well-known v-chevron formation in the SS FLC. As compared Fig. 2(b) with Fig. 2(c), or Fig. 3(d) with Fig. 3(f), the fine structure and the position of the stripe is slightly different between them besides the increase in the contrast of the stripe texture. It seems that the clear stripe in Fig. 2(c) is related to the defects (white spots).

The appearance of the in-plane layer deflection or the h-chevron characterizes the layer structure in the SmA and SmC_A^{*} phases of this AFLC material, compared to the v-chevron preference in SmC^{*} of FLC materials [10]. The origin of the in-plane layer deflection is discussed in the following. Since most of the stripe seems to relate to the white defect (focal conics) as shown in Figs. 3(e) and (f), geometrical constraint might play a role to realize the h-chevron. Once the h-chevron is generated, it is easy to propagate along the rubbing direction similar to the needle defect generation and propagation in SmC^{*} [15, 16]. Another possibility for the h-chevron generation is the surface electroclinic effect exerting on surface molecules, since the surface field is normal to the surface [17]. Furthermore, it is not excluded that the memory effect of the h-chevron of the low temperature phase remains

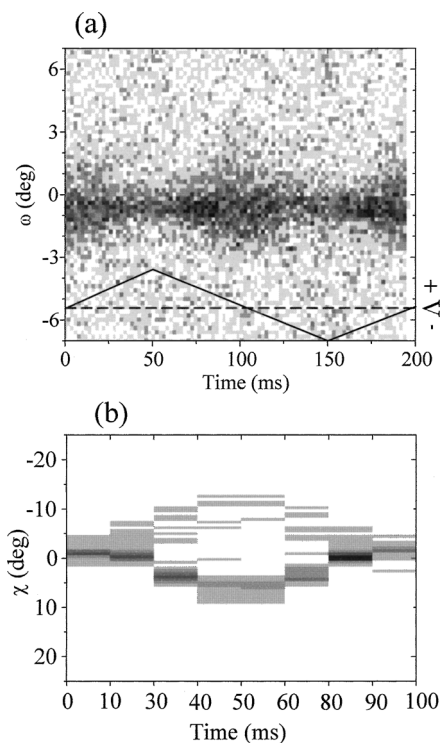


FIGURE 8 Time resolved ω -profile (a) for the triangular wave form (5 Hz, ± 60 V) and the χ -profile (b) for a half cycle of the same wave form. An inset in (a) shows the change in the applied voltage during measurements. The profile (b) was obtained at $\omega = -0.6^\circ$. 1 ms and 10 ms time resolution for (a) and (b), respectively.

in SmA; since the sample was set to the stage after the off-line sample preparation and was carefully heated from the room temperature, the X-ray measurement was performed for the sample subjected to SmC* sub-phases and the crystalline phase.

In the electroclinic effect, the reversible transition between the bookshelf and the h-chevron occurs. The time resolved χ -profile (Fig. 8(b)) is quite similar to the dynamic layer response observed in the SmC* variants under the high field [10]. The h-chevron generation seems to be consistent with the previous macroscopic observation [13, 14] while the weak tail appeared in the ω -profile (Fig. 6(c)) suggests the existence of the v-chevron. Further experiments are now underway.

From Figs. 6(c) and (d), the effect of the electric field on the stripe is just the enhancement of the existing one. After the electric field is turned off (Figs. 6(e) and (f)), the texture is quite similar to the initial ones (Figs. 6(a) and (b)). The surface molecule seems to remain nearly at the same position and in the same alignment during the field application. This is also consistent with the time-resolved measurement in Figs. 8(a) and (b), where the bookshelf structure is realized at the low field.

Acknowledgement

The authors would like to thank the staff of PF for their help during experiments. We wish to thank Professor K. Sekizawa, Professor Y. Takano and Dr. K. Takase for their continuous encouragement during the study. This work was carried out under the approval of the Photon

Factory Advisory Committee (Proposal No. 98G341 and 00G279). This work was partly supported by Grant-In-Aid for Scientific Research on Priority Area (B) (12129202 and 12129206), the Ministry of Education, Science, Sports and Culture.

References

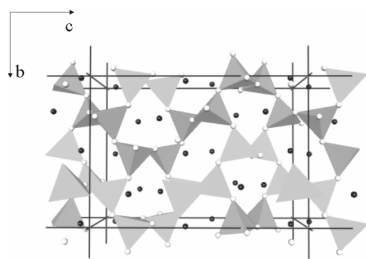
1. S. T. Lagerwall, *Ferroelectric and Antiferroelectric liquid crystals* (Wiley, Weinheim, 1999).
2. I. Musevic, R. Blinc, and B. Zeks, *The Physics of Ferroelectric and Antiferroelectric Liquid Crystals* (World Scientific, 2000).
3. M. Johno, Y. Ouchi, H. Takezoe, A. Fukuda, K. Terashima, and K. Furukawa, *Jpn. J. Appl. Phys.* **29**, L111 (1990).
4. L. S. Matkin, H. F. Gleeson, L. J. Bayliss, S. J. Watson, N. Bowring, A. Seed, M. Hird, and J. W. Goodby, *Appl. Phys. Lett.* **77**, 340 (2000).
5. S. J. Watson, L. S. Matkin, L. J. Bayliss, N. Bowring, H. F. Gleeson, M. Hird, and J. Goodby, *Phys. Rev. E* **65**, 31705 (2002).
6. P. Cluzeau, P. Barois, H. T. Nguyen, and C. Destrade, *Eur. Phys. J. B* **3**, 73 (1998).
7. P. Cluzeau, P. Barois, and H. T. Nguyen, *Eur. Phys. J. E* **7**, 23 (2002).
8. Y. Takahashi, A. Iida, Y. Takanishi, T. Ogasawara, K. Ishikawa, and H. Takezoe, *Jpn. J. Appl. Phys.* **40**, 3294 (2000).
9. Y. Takahashi, A. Iida, Y. Takanishi, T. Ogasawara, K. Ishikawa, and H. Takezoe, *Mol. Cryst. Liq. Cryst.* **365**, 853 (2001).
10. Y. Takahashi, A. Iida, Y. Takanishi, T. Ogasawara, M. Nakata, K. Ishikawa, and H. Takezoe, *Phys. Rev. E* **67**, 051706 (2003).
11. Y. Suzuki, T. Hagiwara, I. Kawamura, N. Okamura, T. Kitazume, M. Kakimoto, Y. Imai, Y. Ouchi, H. Takezoe, and A. Fukuda, *Liq. Cryst.* **6**, 167 (1989).
12. A. Suzuki, H. Orihara, Y. Ishibashi, Y. Yamada, N. Yamamoto, K. Mori, K. Nakamura, Y. Suzuki, T. Hagiwara, I. Kawamura, and M. Fukui, *Jpn. J. Appl. Phys.* **29**, L336 (1990).
13. A. G. Rappaport, P. A. Williams, B. N. Thomas, N. A. Clark, M. B. Ros, and D. M. Walba, *Appl. Phys. Lett.* **67**, 362 (1995).
14. R. E. Geer, S. J. Singer, J. V. Selinger, B. R. Ratna, and R. Shashindhar, *Phys. Rev. E* **57**, 3059 (1998).
15. R. F. Shao, P. C. Willis, and N. A. Clark, *Ferroelectrics* **121**, 127 (1991).
16. Y. Takanishi, A. Iida, K. Ishikawa, H. Takezoe, and A. Fukuda, *Jpn. J. Appl. Phys.* **38**, 4132 (1999).
17. K. Nakagawa, T. Shinomiya, M. Koden, K. Tsubota, T. Kuratate, Y. Ishii, F. Funada, M. Matsuura, and K. Awane, *Ferroelectrics* **85**, 39 (1988).

SYNTHESIS AND STRUCTURE OF CaSiN₂

F. Ottinger R. Nesper

ETH Zurich Laboratorium Fur Anorganische Chemie Wolfgang-Pauli-Strasse
10 Hci H106 ZURICH 8093 SWITZERLAND

Containing corner-sharing as well as edge-sharing Si₄-tetrahedra as the main building blocks, very complex Si-N-networks are possible in ternary nitridosilicates. Therefore the structures of nitridosilicates are a significant extension to the structures found in the family of oxosilicates. Although the synthesis of CaSiN₂ has been reported in the 1960s, the structure of CaSiN₂ has not yet been clarified. Ca₇Si₄N₁₀ was received as the main product by reaction of CaSi₂ and Ca₃N₂ at temperatures of 1400 °C in sealed Niobium ampoules. Crystals of transparent, orange CaSiN₂ were obtained as a by-product. These crystals are embedded in a Calcium matrix, as it is not possible to synthesize them stoichiometrically from only CaSi₂ and Ca₃N₂. Moreover, Calcium is acting as a flux and enables the formation of large single crystals. CaSiN₂ crystallizes in the orthorhombic space group *Pbca* (No. 61) with *a* = 5.129(3) Å, *b* = 10.224(1) Å, *c* = 14.821(4) Å, *Z* = 1, R(*F*_o) = 0.0341. CaSiN₂ is isotopic with KFeO₂ and KGaO₂ building a 3-dimensional network of SiN₄-tetrahedra forming sechser rings. All Si-N[2] distances are within the usual range for nitrido-silicates between 1.719 (6) - 1.778 (6) Å. The Calcium-Calcium distance is 3.052 (1) Å.



Keywords: NITRIDO SILICATES, NETWORK STRUCTURE, HIGH TEMPERATURE SYNTHESIS

11x

OBSERVATION OF DYNAMIC LOCAL LAYER RESPONSE OF
SMECTIC LIQUID CRYSTALS BY X-RAY MICRO-DIFFRACTIONA. Iida¹ Y. Takahashi² Y. Takanishi³ M. Nakata³ K. Ishikawa³ H. Takezoe³High Energy Accelerator Research Organization Institute of Materials
Structure Science 1-1 O-Ho TSUKUBA IBARAKI 305-0801 JAPAN¹Photon Factory, Institute of Materials Structure Science, High Energy
Accelerator Research Organization ²The Graduate University for Advanced
Studies ³Department of Organic and Polymer Materials, Tokyo Institute of
Technology

For the direct determination of the microscopic local layer structure in the smectic liquid crystal, the synchrotron X-ray microbeam diffraction technique becomes a powerful tool[1]. The dynamic local layer response of the stripe texture, which appears in the anti-ferro and ferroelectric liquid crystal (AFLC and FLC), was measured in detail under the high electric field.

The experiment was performed at the Photon Factory (BL4A) by the X-ray beam. The diffracted intensities were measured as functions of angles, which correspond to the layer orientation with respect to the normal to the rubbing direction and the surface normal, respectively. The time resolved measurements were carried out with the time resolution from a few fYs to ms. The samples used were TK-C101(FLC) and TPMHPOBC (AFLC). The layer responses in the SmC* and SmCa phase were measured for FLC and AFLC, respectively. The electroclinic effect is also measured in the SmA phase of both materials. For FLC cells, the reversible local layer change from the horizontal chevron to the quasi-bookshelf structure was confirmed under the triangular waveform. It was shown that the anchoring effect at the alignment film played an important role for the layer transformation. The local layer relaxation time for the step waveform was dependent on the applied electric field and the sample (AFLC/FLC). The relation of the layer response among samples and phases was discussed.

References

[1] Y. Takahashi et al, Jpn. J. Appl. Phys. 40(2001)3294

Keywords: SMECTIC LIQUID CRYSTAL, X-RAY MICROBEAM, TIME-RESOLVED MEASUREMENT

CRYSTAL AND MAGNETIC STRUCTURES OF LAYERED
Sr₂MnGaO_{5+x} OXIDESA.M. Balagurov¹ V.Yu. Pomjakushin¹ A.M. Abakumov² E.V. Antipov² M.V. Lobanov² P. Fischer³ D.V. Sheptyakov^{1,3}¹Joint Institut for Nuclear Research Frank Laboratory of Neutron Physics
Frank Laboratory of Neutron Physics Joint Institut for Nuclear Research
DUBNA MOSCOW REG. 141980 RUSSIA ²Department of Chemistry,
Moscow State University, 119899 Moscow ³Laboratory of Neutron Scattering,
ETHZ&PSI, CH-5232 Villigen, Switzerland

Crystal and magnetic structures of new complex manganese oxides Sr₂GaMnO_{5+x} (*x* = 0, 0.4 and 0.5) were studied by neutron powder diffraction. The crystal structure of the compound with *x* = 0 belongs to a brownmillerite type and consists of alternating SrO, MnO₂, SrO and GaO_{1+x} layers with *Ima2* space symmetry. Mn magnetic moments are aligned antiferromagnetically in all directions below *T*_N=180 K (G-type order). The oxidized compound with *x* = 0.5 has a perovskite-like crystal structure with a tetragonal unit cell of *P4/mmm* space symmetry. The GaO_{1+x} layers are partially filled. Its magnetic structure (*T*_N = 108 K) preserves AFM ordering within the MnO₂ plane, however, the interlayer coupling becomes ferromagnetic (C-type order). The average crystal structure of *x* = 0.4 sample can be satisfactorily described in monoclinic *P2/m* space group but two-phase state could not be excluded. The latter is indicated by two-step magnetic phase transition: appearance G-type structure at 140 K and then C-type structure at 110 K. Despite the distances between neighbouring in-plane and out-of-plane Mn atoms are very different (3.8 Å and 8 Å, respectively) a magnetic structure of all compounds has a 3D character.

Keywords: MANGANITES, LAYERED STRUCTURE, NEUTRON DIFFRACTION

DETERMINATION OF PHASES AND PHASE TRANSITIONS IN
LIQUID CRYSTALSA.K. Schaper¹ Z. Zhao¹ W. Ruland¹ B. Albert²¹Philipps University Materials Science Center Dept of Geosciences Hans-
Meerwein-Str. MARBURG 35032 GERMANY ²Department of Chemistry,
Justus Liebig University, 35392 Giessen, Germany

From certain liquid crystal (LC) compounds it is known that they pass through an intermediate hexatic-B (SmBHex) phase during transition from the crystalline smectic-B (SmB) phase to the liquid-like smectic-A (SmA) phase. This hexatic phase is characterized by long-range bond orientational order over macroscopic dimensions, but only short-range positional order propagating over not more than a few tens of nanometers. The hexagonal bond orientational order correlations extend over a three-dimensional stack of two-dimensional hexatic layers which exhibit only weak interlayer coupling. In this paper, direct proof of the hexatic order in a cyclohexyl derivative of a biphenylic type compound is provided by *in situ* low-dose selected area electron diffraction (SAED). Further information on the phase transitional behavior of the LC material with the bulk transition sequence SmB - SmBhex - SmA - N - I is gained from light microscopy observations, calorimetric measurements, small and wide angle x-ray scattering (SAXS, WAXS), and from x-ray density fluctuation measurements, in particular. The particle density fluctuation of condensed matter is caused by thermal motion of the atoms or molecules, and is influenced in a definite manner by the presence of structural defects and lattice disorder. Therefore, the relationship between the density fluctuation and the x-ray scattering intensity extrapolated toward zero angle may serve as quantitative measure of the state of order and of the strength of particular defect populations in solids. For the first time, we apply this method to characterizing the phase transitional behavior of an LC material.

Keywords: LIQUID CRYSTALS PHASE TRANSITIONS
DIFFRACTION AND SCATTERING



Time resolved X-ray micro-diffraction measurements of the dynamic local layer response to electric field in antiferroelectric liquid crystals

Yumiko Takahashi^a, Atuso Iida^{b,*}, Yoichi Takanishi^c, Toyokazu Ogasawara^c,
Hideo Takezoe^c

^a *The Graduate University for Advanced Studies, 1-1 O-ho, Tsukuba 205-0801, Japan*

^b *Photon Factory, Institute of Materials Structure Science, High Energy Accelerator Research Organization,
1-1 O-ho, Tsukuba, Ibaraki 305-0801, Japan*

^c *Department of Organic and Polymeric Materials, Tokyo Institute of Technology, O-okayama, Meguro-ku, Tokyo 152-8552, Japan*

Abstract

The time-resolved synchrotron X-ray microbeam diffraction experiment has been carried out to reveal the local layer response to the electric field in the antiferroelectric liquid crystal. The X-ray microbeam of a few μm spatial resolution was obtained with Kirkpatrick–Baez optics. The time-resolved small angle diffraction experiment was performed with a time resolution ranging from 10 μs to a few ms. The reversible local layer change between the horizontal chevron and the quasi-bookshelf structure was confirmed by the triangular wave form. The transient layer response for the step form electric field was observed. The layer response closely related with an electric field induced antiferroelectric to ferroelectric phase transition. © 2001 Elsevier Science B.V. All rights reserved.

Keywords: Synchrotron X-ray microbeam; Antiferroelectric liquid crystal; Time-resolved measurements; X-ray micro-diffraction

1. Introduction

Antiferroelectric liquid crystals (AFLC) have attracted much attention from the application point of view and also from the basic interest in the mesophase [1]. Though the macroscopic layer ordering in AFLC can be characterized by the conventional small angle diffraction technique [2], the X-ray microbeam is necessary to investigate

the local layer structure in the texture observed by an optical microscope. The time-resolved experiment is also needed to reveal the layer response to the electric field [3].

The synchrotron X-ray microbeam diffraction has been successfully applied to the characterization of various textures in the thin surface stabilized ferroelectric liquid crystals (FLC) [4–6]. Though the stripe texture observed in AFLC, which runs parallel to the rubbing direction, is important for understanding the electric field induced phase transition between AFLC and FLC phases [7,8], the detailed microscopic local

*Corresponding author. Tel.: +81-298-64-5634; fax: +81-298-64-2801.

E-mail address: atsuo.iida@kek.jp (A. Iida).

layer structure has not yet been clarified. Furthermore, direct evidence of the dynamic local layer response of AFLC to the electric field has not been reported, though the molecular response has been investigated by the optical technique [9].

In this paper, the time-resolved X-ray micro-diffraction technique is described and the results are presented for the time-dependent local layer response in the stripe texture of AFLC.

2. Experimental

The X-ray microbeam system at the Photon Factory (PF) on BL-4A consists of a multilayer monochromator and Kirkpatrick–Baez focusing optics [10,11] (Fig. 1(a)). Owing to the emittance upgrade of the PF 2.5 GeV ring, the focused beam size was reduced from $5 \times 6 \mu\text{m}^2$ (former) to $3 \times 4 \mu\text{m}^2$ (present). The setup around the sample cell is shown in Fig. 1(b). A position sensitive proportional counter (PSPC) was used. The diffracted intensity was measured as a function of ω and χ angle. The ω angle corresponds to the layer tilt angle with respect to the rubbing direction in the cell surface plane, while the χ angle is that with respect to the rubbing direction around the cell surface normal. The ω intensity profile was obtained by rotating the sample around Y -axis, while the χ -intensity profile was obtained simultaneously by the PSPC at a fixed ω angle.

The sample used was TFMHPOBC¹ (AFLC) and was sandwiched between ITO-coated glass plates rubbed one side after alignment film coating. The sample thickness was about $5 \mu\text{m}$. The sample temperature was kept at $T_c - 10^\circ$ during experiments, where T_c was the critical temperature of the phase transition from SmA to SmC_A^{*} (antiferroelectric phase). Due to the limited space around the sample, the sample cell was simply inserted in Cu plates in which a thermofoil heater and a thermocouple were embedded.

The two types of electric fields, i.e. the triangular and step wave form, were applied to the sample

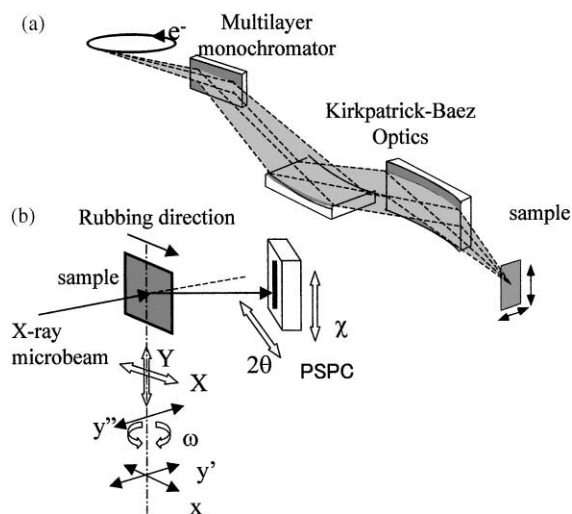


Fig. 1. Schematic representation of the experimental arrangement. (a) X-ray focusing system and (b) the experimental setup around a sample.

cell. Under the triangular field of a sufficiently low frequency, the local layer response is expected to be quasi-static. For the step field (one period consists of four constant voltages of equal time interval, $50 \text{ V} \rightarrow 0 \text{ V} \rightarrow -50 \text{ V} \rightarrow 0 \text{ V}$), the transient local layer response for the field induced phase transition can be measured. The high-to-low electric field change corresponds to the ferroelectric to antiferroelectric transition and vice versa. The gate signal from a function generator via a delay pulser was applied to a router of a multichannel analyzer (time-resolved χ -profile). With this mode, eight sampling points in a period can be measured. The signals were successively accumulated during the collection time at each ω -angle. A multichannel scaler was used to measure the time-resolved ω -intensity profile (MCS mode) and was controlled by the same trigger signal from the function generator. Depending on the response time of the local layer to the electric field, the time resolution from $10 \mu\text{s}$ to a few ms was used.

3. Results and discussion

Typical local layer structures in the AFLC cells are the vertical chevron (v-chevron) and the

¹ 4-(1-trifluoromethylheptyloxycarbonyl)phenyl-4'-octyloxy-biphenyl-4-carboxylate.

horizontal chevron (h-chevron) as shown in Fig. 2(a). A pair of peaks is expected for ω -profile and χ -profiles due to the v-chevron and the h-chevron, respectively. The horizontal chevron (h-chevron) is considered to be related with the stripe texture.

In the initial state of SmC_A^* phase, the layer structure was a combination of the v-chevron and the h-chevron. When the triangular electric field was increased, the layer structure changed irreversibly to the h-chevron. Time integrated χ profiles shown in Fig. 2(b) were obtained by changing the analyzing position perpendicular to the stripe texture. The alternative intensity modulation in the χ -profile ($\sim 10 \mu\text{m}$ period) clearly indicates the structure modulation in the stripe texture. A series of ω -profiles showed the v-bookshelf structure independent of the analyzing position.

For time-resolved microbeam X-ray diffraction profiles with triangular wave form, the reversible local layer change between the horizontal chevron and the quasi-bookshelf structure was confirmed. The peak intensity of the ω -profile and the h-chevron angle in the χ -profile showed the hysteresis corresponding to the field-induced ferroelectric to antiferroelectric phase transition [12].

The transient layer response was obtained for the step form electric field. Fig. 3 shows the time

resolved χ -profile for the high (50 V) to low (0 V) step form electric field measured at $\omega = -1.3^\circ$, which is the bookshelf peak position in the ω -profile. The initial h-chevron angle ($\alpha \sim 2.5^\circ$) decreases as a function of time. The layer structure is again the h-chevron after 5.3 ms (or 0.3 ms after field change) and the h-chevron angle becomes slightly large ($\alpha \sim 3.5^\circ$). The transient time from the ferroelectric to antiferroelectric phases was about 0.3 ms in the present cell. Though the response time of sub-ms seems to correspond to the slow process due to the domain motion observed by the optical response [9], the positional dependence of the transient time was not confirmed in the present experiment. For the low (0 V) to high (50 V) step wave form, the layer response was much faster (less than 40 μs). The difference in the transient time between above process reflects the difference in the driving force of the phase transition.

In conclusion, the time-resolved micro-diffraction experiment revealed the local layer structure

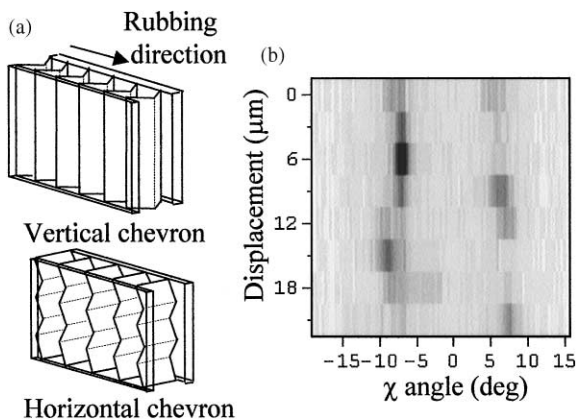


Fig. 2. (a) The vertical chevron and the horizontal chevron local layer structures of the (anti-) ferroelectric phase. (b) A series of time integrated χ intensity profiles during a triangular electric field application (5 Hz, ± 50 V) as a function of the vertical displacement across the stripe texture with $3 \mu\text{m}/\text{step}$. χ -profiles were obtained at $\omega = 0.4^\circ$.

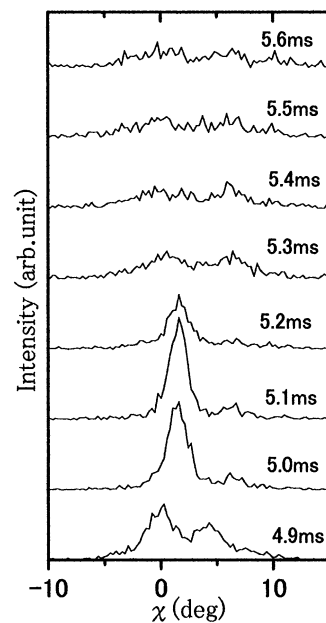


Fig. 3. The time-resolved X-ray diffraction χ -intensity profiles for the high (50 V) to low (0 V) electric field obtained at $\omega = 0.3^\circ$. The field change from high to low occurred at 5 ms. Time resolution was 0.1 ms.

and its response to the electric field in the AFLC for the first time. The quantitative analysis of the layer response and its dependence on the sample preparing process are now underway.

This work was carried out under the approval of the Photon Factory advisory committee (Proposal No. 98G341).

References

- [1] S.T. Lagerwall, *Ferroelectric and Antiferroelectric Liquid Crystals*, Wiley-VHC, Weinheim, 1999.
- [2] M. Johno, Y. Ouchi, H. Takezoe, A. Fukuda, K. Terashima, K. Furukawa, *Jpn. J. Appl. Phys.* 29 (1990) L111.
- [3] A. Morse, H.F. Gleeson, *Mol. Cryst. Liq. Cryst.* 302 (1997) 121.
- [4] A. Iida, T. Noma, H. Miyata, *Jpn. J. Appl. Phys.* 35 (1996) 160.
- [5] Y. Takanishi, A. Iida, K. Ishikawa, H. Takezoe, A. Fukuda, *Jpn. J. Appl. Phys.* 38 (1999) 4132.
- [6] A. Iida, T. Noma, H. Miyata, *Jpn. J. Appl. Phys.* 38 (1999) 2845.
- [7] J. Pavel, M. Glogarova, *Ferroelectrics* 113 (1991) 619.
- [8] K. Ito, M. Johno, Y. Takanishi, Y. Ouchi, H. Takezoe, A. Fukuda, *Jpn. J. Appl. Phys.* 30 (1991) 735.
- [9] M. Johno, K. Itoh, J. Lee, Y. Ouchi, H. Takezoe, A. Fukuda, T. Kitazume, *Jpn. J. Appl. Phys.* 29 (1990) L107.
- [10] A. Iida, T. Noma, *Nucl. Instr. Meth. B* 82 (1993) 129.
- [11] A. Iida, T. Noma, K. Hirano, *Ferroelectrics* 149 (1993) 117.
- [12] Y. Takahashi, A. Iida, Y. Takanishi T. Ogasawara, K. Ishikawa, H. Takezoe, *Jpn. J. Appl. Phys.*, submitted.